Extrahypothalamic GABAergic nociceptin-expressing neurons regulate AgRP neuron activity to control feeding behavior

Smith, Mark A ; Choudhury, Agharul I ; Glegola, Justyna A ; Viskaitis, Paulius ; Irvine, Elaine E ; De Campos Silva, Pedro Caldas Custodio ; Khadayate, Sanjay ; Zeilhofer, Hanns Ulrich ; Withers, Dominic J

Abstract: Arcuate nucleus agouti-related peptide (AgRP) neurons play a central role in feeding and are under complex regulation by both homeostatic hormonal and nutrient signals and hypothalamic neuronal pathways. Feeding may also be influenced by environmental cues, sensory inputs and other behaviors implying the involvement of higher brain regions. However, whether such pathways modulate feeding through direct synaptic control of AgRP neuron activity is unknown. Here we show that nociceptin-expressing neurons in the anterior bed nuclei of the stria terminalis (aBNST) make direct GABAergic inputs onto AgRP neurons. We found that activation of these neurons inhibited AgRP neurons and feeding. Activity of these neurons increased upon food availability and their ablation resulted in obesity. Furthermore, these neurons received afferent inputs from a range of upstream brain regions as well as hypothalamic nuclei. Therefore, aBNST nociceptin/GABAergic neurons may act as a gateway to feeding behavior by connecting AgRP neurons to both homeostatic and non-homeostatic neuronal inputs.

DOI: https://doi.org/10.1172/JCI130340

JCI The Journal of Clinical Investigation

Extrahypothalamic GABAergic nociceptin-expressing neurons regulate AgRP neuron activity to control feeding behavior

Mark A. Smith, … , Hanns Ulrich Zeilhofer, Dominic J. Withers

J Clin Invest. 2019. https://doi.org/10.1172/JCI130340.

Research In-Press Preview Metabolism Neuroscience

Graphical abstract

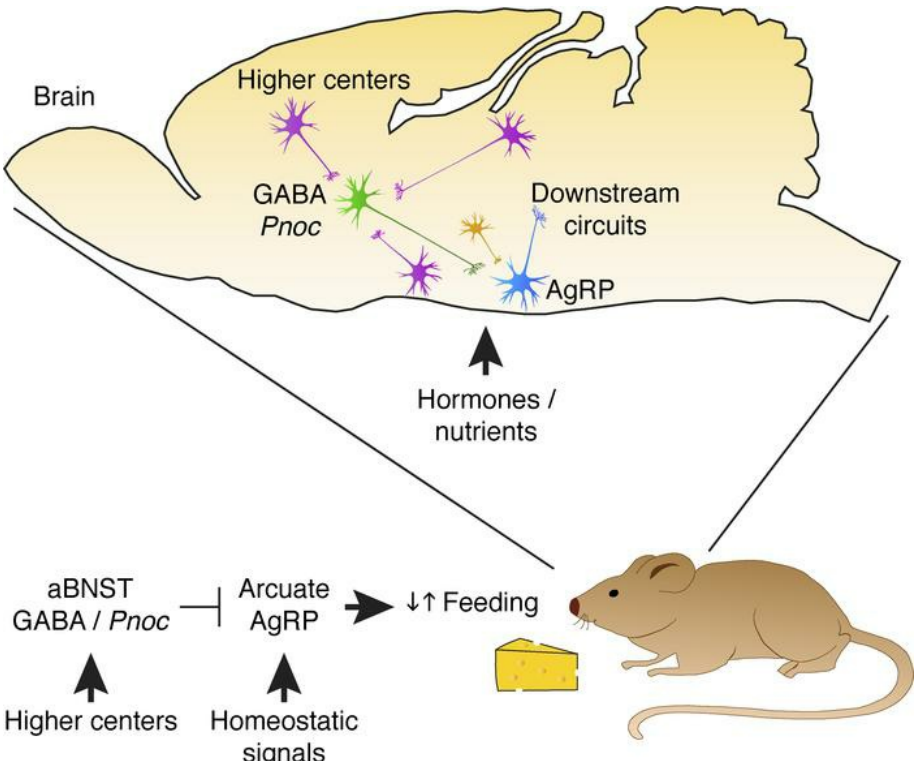

Find the latest version:

http://jci.me/130340/pdf

Extrahypothalamic GABAergic nociceptin-expressing neurons regulate AgRP neuron activity to control feeding behavior

Mark A. Smith[1*], Agharul I. Choudhury[2], Justyna A. Glegola[2], Paulius Viskaitis[2,#], Elaine E. Irvine[2], Pedro Caldas Custodio de Campos Silva[2], Sanjay Khadayate[2], Hanns Ulrich Zeilhofer[3], Dominic J. Withers[1,2*]

1. Institute of Clinical Sciences, Faculty of Medicine, Imperial College, London W12 0NN. UK
2. MRC London Institute of Medical Sciences, London, W12 0NN. UK
3. Institute of Pharmacology and Toxicology, University of Zurich, Winterthurerstrasse 190, CH-8057 Zurich, and Institute of Pharmaceutical Sciences, Swiss Federal Institute of Technology (ETH) Zurich, Vladimir-Prelog-Weg 1-5/10, CH-8093 Zurich, Switzerland.

Current address: Institute of Neuroscience, Swiss Federal Institute of Technology (ETH) Zurich, Schorenstrasse 16, CH-8603 Schwerzenbach, Switzerland.

*** Correspondence**

d.withers@imperial.ac.uk and mark.smith@imperial.ac.uk

Contact addresses:

Professor Dominic J. Withers
Metabolic Signalling Group
MRC London Institute of Medical Sciences
Room 3013A, Clinical Research Building
Imperial College London
Hammersmith Campus
W12 0NN
UK
Tel: +44 (0)208 383 3014
Email: d.withers@imperial.ac.uk

Dr Mark A. Smith
Metabolic Signalling Group
Institute of Clinical Sciences
Room 3013A, Clinical Research Building
Imperial College London
Hammersmith Campus
W12 0NN
UK
Tel: +44 (0)208 383 8583
Email: mark.smith@imperial.ac.uk

The authors have declared that no conflict of interest exists.

Our funding agency requires a Creative Commons CC-BY license in order to support publication fees for this manuscript.

Abstract

Arcuate nucleus agouti-related peptide (AgRP) neurons play a central role in feeding and are under complex regulation by both homeostatic hormonal and nutrient signals and hypothalamic neuronal pathways. Feeding may also be influenced by environmental cues, sensory inputs and other behaviors implying the involvement of higher brain regions. However, whether such pathways modulate feeding through direct synaptic control of AgRP neuron activity is unknown. Here we show that nociceptin-expressing neurons in the anterior bed nuclei of the stria terminalis (aBNST) make direct GABAergic inputs onto AgRP neurons. We found that activation of these neurons inhibited AgRP neurons and feeding. Activity of these neurons increased upon food availability and their ablation resulted in obesity. Furthermore, these neurons received afferent inputs from a range of upstream brain regions as well as hypothalamic nuclei. Therefore, aBNST nociceptin/GABAergic neurons may act as a gateway to feeding behavior by connecting AgRP neurons to both homeostatic and non-homeostatic neuronal inputs.

Introduction

Feeding requires the integration of multiple neuronal networks to elicit appropriate behavioral and metabolic responses (1-3). These networks are sensitive to a range of modulatory inputs including nutrients and hormones, the reward value of food, environmental cues and internal emotional state (1-3). While multiple anatomically-defined regions and chemically-defined neurons control feeding, hypothalamic arcuate nucleus agouti-related protein (AgRP) and neuropeptide-Y (NPY)-expressing neurons play a central role in feeding and related behaviors (4-6). AgRP/NPY neurons are themselves under complex regulation by peripheral hormonal and nutrient signals and by neuronal inputs including those from the paraventricular hypothalamus (PVN) and dorsomedial nucleus of the hypothalamus (DMH) (1-3, 7, 8). AgRP/NPY neuronal excitability increases during nutrient deficiency and falls upon food presentation and consumption with specific post-ingestive signals and intrahypothalamic circuits involved (7, 9-13). A range of other inputs such as sensory cues, reward signals, stress, learning and memory impact upon AgRP/NPY neuron activity implying that they may also be regulated by neuronal circuits from outside the hypothalamus (7, 10, 13, 14). However, to date no extrahypothalamic afferent pathways have been identified that directly synaptically regulate AgRP/NPY neuron activity and thence feeding. Therefore, we set out to explore potential circuits that might directly regulate AgRP/NPY neurons focusing on the bed nuclei of the stria terminalis (BNST) as neuronal tracing studies have suggested anatomical connections to the arcuate nucleus and the BNST is involved in appetitive feeding behaviors (15-21).

Here, we show that anterior BNST (aBNST) neurons co-expressing GABA and the opioid-like peptide nociceptin, i) inhibit arcuate AgRP/NPY neurons via GABAergic transmission to suppress food intake independent of changes in anxiety, ii) show increases in

endogenous activity at the initiation of feeding temporally consistent with the reduction in AgRP/NPY activity, iii) regulate bodyweight and iv) receive afferent inputs from a range of upstream brain regions. These studies thus identify GABAergic aBNST nociceptin neurons as a previously unrecognized extrahypothalamic neuronal population that regulates food intake and bodyweight via AgRP/NPY neurons by acting as a potential feeding gateway to link both homeostatic and non-homeostatic inputs.

Results

GABAergic neurons in the aBNST directly inhibit arcuate NPY neurons

Anatomical tracing studies have identified axons that project from the anteromedial BNST (amBNST) towards the arcuate nucleus (16, 20, 21). To investigate the function of these projections, we performed virus-based tracing experiments. As BNST neurons are predominantly GABAergic (22), we injected adeno-associated viral (AAV) particles containing a cre-dependent channelrhodopsin-2-mCherry (ChR2-mCherry) construct into the aBNST of mice expressing cre-recombinase driven by the vesicular GABA transporter (*Slc32a1* or Vgat-Cre) to selectively transduce GABAergic neurons (Figure 1A). Expression of mCherry in somas and fibers was observed surrounding the anterior commissure thus capturing the various sub-nuclei of the aBNST (Figure 1B). Furthermore, mCherry-containing projection fibers were also observed in a number of brain regions with particularly dense expression in the arcuate nucleus (Figure 1C and data not shown). We did not find mCherry expressing somas in the arcuate nucleus suggesting that aBNST injected viral particles of the AAV1 serotype did not retrogradely label neurons in the arcuate nucleus.

To examine if these aBNST axons made direct synaptic connections with specific arcuate nucleus neurons that regulate feeding, we injected ChR2-mCherry AAV into the aBNST of Vgat-Cre mice that were crossed with either *Pomc*-topaz GFP (*Pomc*-GFP) or *Npy*-renilla GFP (*Npy*-hrGFP) transgenic mice to identify arcuate pro-opiomelanocortin (POMC) or NPY neurons, respectively. Arcuate nucleus slices that did not contain the BNST but retained ChR2-mCherry expressing axons from the aBNST, were prepared for ex vivo ChR2-assisted circuit mapping (Figure 1D). Synaptic currents were evoked by 4 ms light pulses and a mean of 80 consecutive trials were used to distinguish photostimulated events from spontaneously occurring synaptic input. An inward current was observed in NPY but not POMC neurons

(Figure 1E and 1F), which when tested was completely blocked by a $GABA_A$ receptor antagonist (n = 3 neurons from 2 mice, Figure 1E). Moreover, using a burst stimulating protocol (10 Hz for 3 s and repeated every 4 s), ChR2-induced synaptic release suppressed spontaneous action potential firing in arcuate NPY neurons (Figure 1G and 1H, Supplemental Figure 1A). These findings indicated a specific inhibitory synaptic connection between GABAergic aBNST neurons and orexigenic AgRP/NPY neurons but not anorexigenic POMC neurons in the arcuate nucleus.

Optogenetic stimulation of GABAergic aBNST fibers in the arcuate nucleus suppresses feeding

To determine if GABAergic aBNST projections to arcuate NPY neurons regulate feeding, cre-dependent ChR2-mCherry or YFP containing AAVs were injected into the aBNST of 4-month old male Vgat-Cre mice and wild-type (WT) littermates with optical fibers positioned above or within the arcuate nucleus (Figure 1I and Supplemental Figure 1B). Two weeks after surgery overnight fasted mice were photostimulated using the same burst protocol as applied in the ex vivo slice studies. Stimulation of ChR2-mCherry expressing aBNST to arcuate nucleus efferent fibers significantly suppressed food intake after 4 hours, an effect which persisted following the cessation of the light stimulus (Figure 1J and 1K). This was not observed in photostimulated WT mice injected with ChR2-mCherry (Supplemental Figure 1C) or in YFP injected Vgat-Cre mice (Supplemental Figure 1D). Stimulation of BNST fibers at a more dorsal site (~0.9 mm from the arcuate nucleus) did not alter feeding in ChR2-mCherry injected WT or Vgat-Cre mice suggesting that the effect was specific to the arcuate nucleus (Supplemental Figure 1E and 1F).

A subset of GABAergic aBNST to arcuate nucleus projection neurons express nociceptin and inhibit NPY neurons

The aBNST displays neurochemical heterogeneity but recent evidence has shown that expression of specific neuropeptides may underlie the functional specificity of BNST GABAergic neuronal populations (23). We therefore sought to define whether a specific subpopulation of GABAergic neurons was connected to arcuate AgRP/NPY neurons and modulated feeding. A number of peptides expressed in BNST neurons are implicated in feeding, many involving effects on stress and anxiety, but we focused our initial studies on two opioid peptides dynorphin and nociceptin. Dynorphin has previously been shown to inhibit NPY neuronal excitability in slice recordings and activation of DMH dynorphin neurons in vivo inhibits AgRP neurons to suppress food intake (7, 24). Arcuate AgRP/NPY neurons express the receptor for nociceptin (called NOP receptor) and exogenous nociceptin inhibits arcuate neurons by the activation of a resting K^+ conductance (25, 26). To explore a potential connection between aBNST dynorphin neurons and AgRP/NPY neurons, we crossed mice expressing cre-recombinase driven by the dynorphin promoter (*Pdyn*-Cre) with *Npy*-hrGFP mice and injected ChR2-mCherry AAV into the aBNST. In agreement with previous studies (27), somas expressing mCherry were observed in the aBNST and axons were present in the arcuate nucleus (data not shown). However, photoexcitation of aBNST dynorphin axons failed to elicit a synaptic response in arcuate NPY neurons (n = 15 neurons from 5 mice, paired t-test, $t(14) = 1.09$, $p = 0.30$) suggesting no functional connection between these neuronal populations.

We then explored the effect of nociceptin on AgRP/NPY neuron excitability. While the inhibitory role of nociceptin on arcuate POMC and gonadotrophin-releasing hormone neurons in electrophysiology studies is documented (26), the actions of nociceptin on AgRP/NPY excitability is less clear. In ex vivo electrophysiology studies, we observed a nociceptin-induced hyperpolarization in arcuate NPY neurons which was associated with a

decrease in input resistance consistent with the activation of a cell membrane conductance (Figure 2A-C). This data therefore suggested the possibility that nociceptin, released from aBNST neurons (that perhaps co-express GABA), inhibits arcuate AgRP/NPY neurons to suppress feeding. However, nociceptin-expressing cells are also found in the ventromedial hypothalamus (VMH) and injection of nociceptin agonists to this brain region increases feeding (28, 29). Therefore, we next investigated whether VMH neurons, which may express and release endogenous nociceptin in the arcuate nucleus, directly synapse with arcuate NPY neurons. Cre-dependent ChR2-mCherry AAV was injected into the VMH of mice expressing cre-recombinase driven by the promoter of steroidogenic factor-1 (Sf1-Cre), which captures the vast majority of VMH neurons, and ex vivo ChR2-assisted circuit mapping was performed. Photostimulation of Sf1 axons produced a robust glutamatergic input to arcuate POMC neurons but this was absent in NPY neurons (Supplemental Figure 2A-C and data not shown). This suggests that VMH glutamatergic neurons, including those that may express nociceptin, do not directly synapse with AgRP/NPY neurons to control their activity and thence feeding.

To investigate if nociceptin-expressing aBNST neurons synapse with arcuate AgRP/NPY neurons, we used a novel BAC transgenic mouse line expressing eGFP under the transcriptional control of the prepronociceptin (*Pnoc*) promoter (*Pnoc*-eGFP). eGFP expression was observed in the aBNST and in other regions such as the septum and preoptic area (Figure 2D) consistent with Allen Brain Atlas (30), our in situ data (Supplemental Figure 3A) and the work of others (31-33). Immunohistochemistry demonstrated that GFP-labelled neurons co-expressed nociceptin in the aBNST (Supplemental Figure 3B). To determine whether *Pnoc*-eGFP neurons in the aBNST co-localized with Vgat-cre neurons, we crossed the *Pnoc*-eGFP and Vgat-Cre mice and injected cre-dependent ChR2-mCherry AAV into the aBNST. Approximately 13% of Vgat-cre neurons expressing mCherry co-localized with *Pnoc*-eGFP in

the aBNST (Figure 2E). Together these findings confirmed the utility of using the *Pnoc*-eGFP mouse to explore the role of aBNST nociceptin neurocircuitry in the regulation of AgRP/NPY neurons.

In order to target *Pnoc*-eGFP neurons with cre-inducible AAV, we used the dependent-on-GFP (DOGCre) method that utilizes GFP-binding proteins to allow the molecular assembly of cre-recombinase on a GFP scaffold thus permitting cre-mediated recombination in cells that express GFP (Figure 3A) (34, 35). A mix of AAVs containing the DOGCre viruses (C-creintG and N-cretrcintG) and cre-dependent ChR2-mCherry were injected into the aBNST of *Pnoc*-eGFP mice. Expression of mCherry in somas was restricted to the aBNST and co-localized completely with GFP expressing neurons (Figure 3B). Ex vivo photostimulation of ChR2-mCherry expressing aBNST neurons induced action potential firing in these cells (Supplemental Figure 4A) and axons expressing mCherry were observed in the arcuate nucleus but to a reduced extent to that seen in the Vgat-Cre mouse studies (Figure 3C and 3D). To determine if these nerve fibers made synaptic connections with arcuate AgRP/NPY neurons, we crossed *Pnoc*-eGFP mice with *Npy*-hrGFP mice and injected DOGCre and ChR2-mCherry or synaptophysin-mCherry AAVs into the aBNST, taking advantage of the fact that the DOGCre technology does not recognize renilla-GFP and thus did not lead to cre-dependent ChR2-mCherry expression in the arcuate nucleus of *Npy*-hrGFP animals (Supplemental Figure 4B and 4C). Synaptophysin-tagged mCherry clustered at the somas of arcuate *Npy*-hrGFP neurons and elsewhere in the mediobasal hypothalamus (Supplemental Figure 4C and 4D). In slice recordings, photostimulation of aBNST nociceptin projections induced an inward current in arcuate *Npy*-hrGFP neurons from both male and female mice (Figure 4A-C). The lack of gender differences with respect to synaptic connectivity suggest that this pathway is not sexually dimorphic. Moreover, when tested, these synaptic currents

were blocked by a $GABA_A$ receptor antagonist (n = 6 neurons from 3 mice, paired t-test, t (5) = 3.21, p = 0.024) confirming the GABAergic nature of these neurons. Furthermore, using a burst pattern of light stimulation, photoexcitation of ChR2-mCherry containing *Pnoc* fibers from the aBNST reduced spontaneous action potential firing rate in arcuate *Npy*-hrGFP neurons (Figure 4D and 4E, Supplemental Figure 4E).

To molecularly characterize BNST *Pnoc* neurons we used the RiboTag method to enrich RNA from these cells (36, 37), subjected this to RNA sequencing and compared this expression profile to that of the whole aBNST. As shown by the volcano plot (Supplemental Figure 5 and accession number GSE135982) 705 genes were enriched and a further 1762 genes were depleted in the aBNST of *Pnoc*-eGFP mice. Prepronociceptin was enriched by 4.97-fold ($p = 1.91e^{-15}$) confirming the selective targeting to *Pnoc* neurons. However, the relative expression levels of several other neuropeptides that are expressed in the BNST (e.g. corticotropin-releasing hormone, *Npy*, somatostatin) were not different. In contrast, the expression of preproenkephhalin (*Penk*) and prodynorphin (*Pdyn*) were depleted (5.33-fold, $p = 4.45e^{-33}$ and 5.59-fold, p = 0.01, respectively) consistent with our ChR2 mapping data that failed to demonstrate a connection between aBNST dynorphin axons and arcuate NPY neurons. Taken together these studies suggest that aBNST nociceptin neurons represent a molecularly distinct GABAergic subpopulation synaptically connected to AgRP/NPY neurons with the potential to regulate feeding behavior.

Optogenetic stimulation Pnoc fibers from the aBNST suppresses feeding but does not elicit anxiety

We next determined if excitation of *Pnoc* fibers from the aBNST could suppress feeding. We injected ChR2-mCherry and DOGCre AAVs into the aBNST of 4-month old male *Pnoc*-eGFP and WT littermate mice and positioned optical fibers within or above the arcuate nucleus (Figure

4F and Supplemental Figure 6A). Photostimulation significantly suppressed feeding after 4 hours in overnight fasted and habituated *Pnoc*-eGFP mice (Figure 4G and 4H) but had no effect on WT mice (Supplemental Figure 6B). In contrast, photostimulation of *Pnoc* nerve axons in dorsal regions (~0.6 mm) from the arcuate nucleus did not alter feeding in WT (Supplemental Figure 6C) or *Pnoc*-eGFP (Supplemental Figure 6D) ChR2-mCherry injected mice. Due to the proximity of the septum to the aBNST, the presence of *Pnoc*-eGFP neurons in this region and studies implicating septal projections in the suppression of feeding (38-40), we injected DOGCre with ChR2-mCherry AAVs into the septum of *Pnoc*-eGFP mice and placed optical fibers in the arcuate nucleus (Supplemental Figure 6E). However, photostimulation of the arcuate nucleus projections did not alter feeding (Supplemental Figure 6F) suggesting that nociceptin-expressing septal neurons that may project to the arcuate nucleus do not regulate food intake.

In view of the role of the aBNST in anxiety-related behaviors, antidromic optogenetic stimulation could alter feeding by changing the affective state of the mouse. To exclude this possibility, we photostimulated ChR2-mCherry expressing aBNST to arcuate nucleus *Pnoc* axons in 4-month old male *Pnoc*-eGFP or WT littermate mice in a novel open-field arena (Figure 5A-E) and in an elevated-zero maze (Figure 5F-H). Mice were continuously photostimulated using the burst protocol for 30 minutes in the open-field task and for 10 minutes on the elevated-zero maze. We observed no differences in the avoidance of the anxiogenic center of the open-field arena, total distance covered or velocity when compared with mice that only expressed DOGCre or were WT (Figure 5C-E). Similarly, time spent in and entrances to the anxiogenic open zones of the elevated-zero maze were not different between ChR2-mCherry expressing mice and littermate controls (Figure 5G and 5H). These

tests suggest that the reduction in feeding is unlikely to be due to an overt anxiety-related behavior.

aBNST Pnoc neurons increase activity during feeding

Next we used fiber photometry to assay endogenous activity of aBNST *Pnoc* neurons in response to food presentation. Given that *Pnoc*-driven eGFP expression would interfere with GFP-based calcium-indicators (e.g. GCamp6), we examined calcium dynamics using a red-florescent calcium-indicator (jRGECO1a) (41). The aBNST of *Pnoc*-eGFP mice was injected with AAV expressing DOGCre and a cre-dependent jRGECO1a construct (Figure 6A). In ex vivo electrophysiological studies, red florescence intensity dynamically increased in response to action potential firing induced by current injections (Figure 6B). Furthermore, spontaneous changes in activity were observed when excited with a 590 nm but not with a 488 nm light source (Figure 6C and 6D) suggesting that endogenous eGFP expression from the *Pnoc* locus does not itself manifest as a dynamic change in florescence. We next implanted optical fibers into the mediodorsal region of the aBNST (Figure 6E and 6F) in view of its reported connectivity with the arcuate nucleus (16). jRGECO1a florescence was stimulated and detected using a modified fiberoptometer. Fasted mice were exposed sequentially to a novel object placed in one pot and followed 10 minutes later by exposure to chow in a second pot (Figure 6G). Florescence ($\Delta F/F$) intensity increased at the initiation of feeding but did not change when mice approached the novel object (Figure 6H) indicating a specific response of aBNST *Pnoc* neurons to food and suggesting they are sensitive to nutritional cues. To confirm that optogenetic stimulation of aBNST *Pnoc* neurons inhibited arcuate AgRP neurons in vivo, we intercrossed *Agrp*-Cre mice with *Pnoc*-eGFP mice and expressed the jRGECO1a reporter in AgRP neurons and ChR2 in aBNST *Pnoc*-eGFP neurons. To exclude potential expression of ChR2 in AgRP neurons, we injected a DOG AAV expressing flp-recombinase (DOG-flpo) and an

flp-dependent rather than cre-dependent ChR2-mCherry (fDIO-ChR2-mCherry) AAV into the aBNST (Figure 6I). Expression of mCherry in the aBNST was co-localized with eGFP expressing neurons and jRGECO1a expression was observed in the arcuate nucleus (Supplemental Figure 7A and 7B). Optical fibers were positioned in the aBNST to photostimulate ChR2 *Pnoc*-eGFP neurons and in the arcuate nucleus to record calcium activity in AgRP neurons (Figure 6I). Mice were habituated to tethering and an open-field arena then ad-libitum fed mice were photostimulated for 2 minutes using the 10 Hz burst stimulation protocol. Consistent with our ex vivo data, excitation of aBNST *Pnoc* neurons reduced AgRP activity in vivo (Figure 6J and 6K).

Chronic ablation of aBNST Pnoc-eGFP neurons increases bodyweight

To gain insights into the long-term physiological consequences upon energy homeostasis of disrupting aBNST *Pnoc* neuron function, we performed caspase-mediated ablation of these neurons (42). We injected the aBNST of 5-month old *Pnoc*-eGFP mice male mice with DOGCre and ChR2-mCherry AAVs with and without a cre-dependent caspase-3 AAV to induce cell-death. Post-mortem analysis (~10 weeks post-injection) confirmed the expression of ChR2-mCherry and by inference cre-recombinase expression (Figure 7A and 7B). Although, mCherry fibers could be observed in the aBNST in both control (Figure 7A) and caspase-3 (Figure 7B) mice, the number of intact somas was reduced by around 75% in the caspase-3 treated mice confirming a significant loss of aBNST *Pnoc* neurons (Figure 8A). In ablated mice, consistent with the time taken for viral expression and cell death, bodyweight increased diverging from control animals after 4 weeks following viral injections (Figure 8B and 8C). Increased bodyweight was associated with adiposity (Figure 8D) but no differences in lean body mass (Figure 8E). Furthermore, caspase treated mice ate more than littermate controls in ad-libitum feeding conditions (Figure 8F). These findings indicate a physiologically relevant role

for the aBNST *Pnoc* to AgRP/NPY neuronal circuitry as loss of the inhibitory effects of this pathway on AgRP/NPY would be anticipated to lead to increased activity of these neurons.

Nociceptin neurons in the aBNST provide a gateway from 'higher centers'

The BNST acts as an integrative center receiving inputs from homeostatic and non-homeostatic higher brain centers. aBNST *Pnoc* neurons might therefore receive inputs relevant to feeding behavior from such areas. Thus, to map presynaptic inputs to aBNST *Pnoc* neurons from such brain regions, we used the glycoprotein-deleted rabies monosynaptic tracing strategy (43). To restrict our mapping to only the aBNST neurons that projected to the mediobasal hypothalamus we took advantage of the absolute requirement for C-creintG and N-cretrcintG to be expressed together to make cre-recombinase using the DOGCre approach (data not shown and (34)). We combined this with packaging the C-creintG construct using the AAV2(retro) serotype (44), which allows retrograde transport from distal axonal arbors such as the arcuate nucleus projecting aBNST *Pnoc* population. To test this approach, initially we injected AAV2(retro) C-creintG into the arcuate nucleus and AAV1 serotyped N-cretrcintG and ChR2-mCherry into the aBNST of *Pnoc*-eGFP mice (Supplemental Figure 8A). This approach ensured that only arcuate nucleus projecting neurons that expressed all 3 viruses would express cre-recombinase and thence ChR2-mCherry. A small number (~10) of florescent neurons were observed in the aBNST (Supplemental Figure 8B) and we reasoned that these hypothalamic projecting aBNST neurons could be used as a seeding population to investigate presynaptic inputs through monosynaptic rabies tracing. Therefore, we injected AAV2(retro) C-creintG into the arcuate nucleus and AAV1 N-cretrcintG into the aBNST of *Pnoc*-eGFP mice to express cre-recombinase. The aBNST was also injected with AAV8 serotyped viral particles containing a cre-dependent avian retroviral receptor (TVA, type-2A) tagged with GFP and AAV1 serotyped cre-dependent N2c-glycoprotein (N2c(G)) with a

nuclear marker (h2BG) and GFP (Figure 9A). After 4 weeks, an EnvA pseudotyped glycoprotein deficient rabies virus (CVS-N2c$^{\Delta G}$) that expressed mCherry was injected into the aBNST and allowed to express for 7 days prior to post-mortem anatomical analysis (43). mCherry expression was observed throughout the aBNST (Figure 9B and 9C) but only co-localized with a small number of GFP neurons which may arise from *Pnoc*-eGFP and/or from the GFP-tagged N2c(G) and TVA constructs (Figure 9B). mCherry expression was also observed in the posterior BNST (pBNST, Figure 9D) consistent with the high degree of synaptic connectivity within this nucleus. We next determined the magnitude of synaptic input by counting the number of mCherry-expressing somas that were present outside the BNST (mean of 3 mice, 1410 ± 423 cells per mouse). The hypothalamus accounted for two thirds of the synaptic input to aBNST *Pnoc* neurons. Substantial inputs were observed from the preoptic area (POA, Figure 9C and Supplemental Figure 8C and 8H), the lateral hypothalamus (LH, Figure 9E and Supplemental Figure 8H) and anterior hypothalamus (AH, Supplemental Figure 8D, 8E and 8H). Expression was also observed at the edges of the PVN (Supplemental Figure 8E and 8H) and in a number of other hypothalamic regions such as the DMH (Supplemental Figure 8F and 8H) and VMH (Supplemental Figure 8G and 8H). Interestingly, the arcuate nucleus displayed very little expression and this was mainly limited to the posterior division. Consistent with known BNST inputs (16, 22, 45-48), the lateral septum (Supplemental Figure 9A and 9G) and the cingulate cortex (Supplemental Figure 9B and 9G) were moderately connected. Lower levels of expression were observed in the subiculum (Supplemental Figure 9C and 9G) which is the major output region of the hippocampus and the retrosplenial cortex (Supplemental Figure 9D and 9G) which has been associated with spatial memory (49). Expression was also observed in the orbital frontal cortex (Supplemental Figure 9E and 9G) and the amygdala but was predominately limited to the medial divisions (Supplemental Figure 9F and 9G). Several

other brain regions also expressed low amounts of mCherry but expression was inconsistent between mice (Supplemental Table 1). Therefore, the aBNST nociceptin population that projects to the arcuate nucleus receives significant inputs from both homeostatic regions in the hypothalamus plus cortical and subcortical inputs that underlie a diverse array of behaviors that may be associated with feeding.

Discussion

The control of feeding by AgRP/NPY neuronal activity is sensitive to many homeostatic influences and the nature of the hormonal and nutrient signals and hypothalamic neurocircuitry underlying such regulation is well explored. It is increasingly recognized that sensory cues, reward signals, stress, learning and memory may also impact upon AgRP/NPY neuron activity (7, 10, 11, 13, 14). However, little is known about the identity and function of the neuronal circuits that may be involved in this control. Here we define a previously unrecognized aBNST neuronal pathway outside of the classical homeostatic circuitry, which directly regulates AgRP/NPY activity, feeding and bodyweight. In addition, these neurons receive inputs from a number of higher brain regions and thus may play a role in coordinating homeostatic and non-homeostatic elements of feeding behavior.

We targeted the aBNST for a number of reasons, i) it receives inputs from a diverse array of brain regions that may be involved in feeding (16, 20, 21), ii) it sends axonal projections to the arcuate nucleus and retrograde mapping of AgRP neurons suggests a connection to the BNST (15, 16) and iii) lesioning studies, local pharmacological manipulation of the BNST and optogenetic control of the aBNST alter bodyweight and feeding (18-20). Our finding that aBNST GABAergic neurons inhibit arcuate AgRP/NPY neurons and suppress food intake now implicates this circuit in the direct regulation of feeding. While in vivo stimulation of aBNST nerve fibers could evoke transmitter release and inhibit other types of neuron in the immediate vicinity of the implanted optical fibers, the observed suppression of food intake is consistent with the phenotype seen with direct or synaptically-induced AgRP/NPY neuronal inhibition (5, 7). aBNST GABAergic neurons have previously been implicated in feeding behavior as optogenetic activation of their projections to LH glutamatergic neurons produced voracious feeding in satiated mice (18). However, subsequent studies have suggested that

this circuitry may have a broader role in appetitive behaviors that is not necessarily specific to food (6, 50). In contrast, our studies identify an aBNST GABAergic pathway that specifically synapses with AgRP/NPY feeding neurons that may provide a direct input from higher brain centers to a key and well-established feeding circuit.

The aBNST is a complex region in terms of cytoarchitecture, synaptic connectivity and the fast transmitters, neuropeptides and receptors that are expressed within the various sub-nuclei (16, 20, 22, 47). Recent evidence has shown that expression of specific neuropeptides may underlie the functional specificity of different BNST GABAergic neuronal populations involved in the regulation of emotional states (23). We were therefore interested to see if such a model may also operate with respect to the GABAergic aBNST population that regulated feeding via AgRP/NPY neurons. The opioid peptides dynorphin and nociceptin were attractive candidates since they are highly expressed in the aBNST and have inhibitory effects on arcuate neuronal populations (24, 26). Our finding that nociceptin but not dynorphin-expressing neurons in the aBNST were synaptically connected to AgRP/NPY neurons suggests that a distinct neurochemically-defined population may indeed regulate this arcuate nucleus population. Consistent with these observations, our RiboTag RNAseq studies demonstrated enrichment of nociceptin and depletion of dynorphin RNAs in these cells further suggesting they are a specific cell-population. Our subsequent in vivo studies demonstrated that optogenetic stimulation of aBNST nociceptin/GABA axons in the arcuate nucleus suppressed food intake consistent with AgRP neuronal inhibition and with our data targeting the whole aBNST GABAergic population. Consistent with these findings, in vivo optogenetic activation of aBNST nociceptin/GABA neurons led to a suppression of AgRP neuron activity suggesting a functional link between these events. Moreover, the ablation of aBNST nociceptin/GABA neurons increased bodyweight and food intake leading to increased adiposity. These changes

while not of the same magnitude, resemble the increases in bodyweight produced by chronic direct modulation of AgRP/NPY neurons which alters feeding and energy expenditure (5). However, in our ablation studies we did not directly assess AgRP neuron activity and so the precise contribution of any disinhibition of AgRP neurons through ablation of aBNST nociceptin neurons remains to be defined.

The findings of an anorexigenic effect upon activation of nociceptin-expressing neurons might seem at odds with the previous literature that describes an increase in feeding when pharmacological doses of nociceptin are delivered either intracerebroventricularly or into specific brain regions such as the arcuate nucleus (20, 28, 51). It has been suggested that this orexigenic effect occurs via inhibition of arcuate POMC and VMH neurons (26, 28, 29). However, injection of neuropeptides is unlikely to resemble the spatial and temporal pattern of physiological release but will instead likely induce long-lasting binding to nociceptin receptors throughout the arcuate nucleus, VMH and other regions. Thus, the physiological outcome of pharmacological nociceptin administration is likely to be an amalgamated phenotype with perhaps the predominant effect when acting at a range of nociceptin target neurons depending on the balance of activity at AgRP and POMC neurons. Indeed, simultaneous ablation of arcuate anorexigenic POMC and orexigenic AgRP/NPY neurons results in mild obesity suggesting a dominance of POMC neurons in such manipulations (52).

Nociceptin is likely to have additional roles in feeding behavior as its administration into the BNST prevents corticotropin-releasing hormone induced stress and anorexia (51). In addition, nociceptin-expressing neurons in the central amygdala (CeA) promote the intake of highly palatable food but not normal chow and nociceptin neurons in the VTA are also involved in reward behavior (53, 54). Intriguingly, CeA nociceptin-expressing neurons project to the ventral aBNST to alter reward and anxiety but not food intake. These findings contrast

with our work on aBNST nociceptin-expressing neurons which showed feeding and bodyweight phenotypes on a chow diet. We also found no effects of the activation of these neurons upon anxiety-like behaviors and our rabies tracing studies revealed limited connection with the CeA or the PVN that forms part of the hypothalamic-pituitary-adrenal axis underlying stress responses (55). Taken together it is likely that the aBNST and CeA nociceptin circuits are distinct pathways regulating different aspects of feeding behavior.

AgRP/NPY neuronal activity drops prior to feeding but the mechanisms underlying this observation and its physiological consequences are complex. The dynamic changes in AgRP/NPY neuronal activity are thought to be primarily due to changes in the circulating levels of hormones and nutrients but are also influenced by sensory signals indicating that anticipatory and perhaps other inputs are involved (7, 9-13). Several processes have been suggested to be mediated by the changes in AgRP/NPY activity including the concept that it provides a negative teaching signal, it suppresses appetitive behaviors and provides a reward signal (7, 10, 13, 14). The rapid reductions in activity seen in homeostatic circuits may also be learned (13). In fiber photometry studies we observed an increase in endogenous aBNST nociceptin neuronal activity when mice began to eat but not when they approached a novel object. These data closely resemble the temporal changes in activity found GABAergic neurons in the DMH and AgRP/NPY neurons which increase and decrease their activity prior to feeding, respectively. Nevertheless, additional molecular studies such as loss of function approaches will be required to determine whether the activity of these presynaptic neurons underlie in part, the reduction in AgRP activity during feeding. Indeed, there is a temporal discrepancy between altered endogenous nociceptin neuron activity (seconds-minutes) and the suppression of food intake (minutes-hours) induced by photostimulation although such differences are likely to be due to our inability to detect small changes in food intake at earlier

time points. In addition, the magnitude and time-course of feeding suppression seen with optogenetic activation of DMH GABAergic neurons is more marked than what we observe with aBNST photostimulation (7). This may suggest that DMH neurons innervate and inhibit arcuate AgRP neurons to a greater extent than aBNST neurons.

To determine if synaptic inputs from other brain regions could provide the anatomical basis for this dynamic shift in activity, we undertook presynaptic tracing studies in aBNST nociceptin/GABA neurons that projected to the arcuate nucleus. We used the AAV2(retro) serotype to express cre-recombinase specifically in aBNST nociceptin/GABA neurons projecting to the mediobasal hypothalamus and then targeted these neurons with a glycoprotein-deficient rabies virus that expressed mCherry in the presynaptic neurons. As anticipated given the high level of interconnectivity within the BNST, we observed significant mCherry expression within both the aBNST and posterior BNST. We also observed significant expression in the hypothalamus with the POA being most connected. Interestingly, there was very little expression in the arcuate nucleus despite the observation that AgRP/NPY neurons project to the aBNST to control feeding suggesting that an alternate aBNST neuronal population may mediate this effect (17). We also observed inputs from the subiculum and septum which are major outputs regions of the hippocampus and could suggest that sensory or spatial memory is influencing the activity of these neurons (16). We also observed significant inputs from the cingulate cortex which is implicated in a range of behaviors including emotion, reward, memory as well as binge eating disorders (56, 57). In contrast, we observed only scattered input from the medial and basomedial amygdala and no input from the basolateral amygdala and very sparse input from sensory cortical and hindbrain regions. This anatomical profile is therefore consistent with the targeting of the medial aBNST rather than the lateral aBNST which would suggest that our approach was effectively capturing the

arcuate nucleus projecting amBNST region (16, 22, 46). It is therefore possible that these additional inputs from higher brain regions may modulate the activity of aBNST nociceptin neurons as mice feed. In turn this would regulate AgRP/NPY neuron activity, allowing these feeding neurons to be sensitive to a wide range of extrahypothalamic inputs. However, the functional significance of these connections has yet to be established and will require further study.

In summary, we have defined a previously unrecognized mechanism by which AgRP/NPY neuronal activity, feeding and bodyweight are modulated by a neuropeptide-defined GABAergic aBNST population. This circuitry is active during feeding and is connected to a range of hypothalamic and higher brain regions and this may permit non-homeostatic brain regions to direct the activity of a key homeostatic neuronal pathway. With a behavior that is as complex as feeding, requiring information from multiple neuronal circuits and homoeostatic inputs, it is important to be able to process this information without losing the fidelity of the key inputs that initiate feeding. We therefore propose that aBNST nociceptin/GABA neurons provide a gateway which integrates non-homeostatic circuits into a single synaptic output that regulates AgRP/NPY neuronal activity and feeding.

Methods

Mice

Vgat-Cre (*Slc32a1*tm2(cre)Lowl/J), *Pdyn*-Cre (B6.129S-*Pdyn*tm1.1(cre)Mjkr/LowlJ), Sf1-Cre (Tg(*Nr5a1*-cre)7Lowl/J), *Agrp*-Cre (*Agrp*tm1(cre)Lowl), *Npy*-hrGFP (B6.FVB-Tg(*Npy*-hrGFP)1Lowl/J) and *Pomc*-GFP (B6.Cg-Tg(*Pomc*-MAPT/Topaz)1RCK/J) were obtained from Jackson Laboratories. Bacterial artificial chromosome (BAC) transgenic mice (Tg(*Pnoc*-eGFP)#Uze) expressing eGFP under the transcriptional control of the *Pnoc* gene were generated using homologous recombination of the BAC and pronucleus injection of the modified BAC into fertilized oocytes. Eight clones of the BAC library RPCI-23 (Research Genetics) containing exon 2 of the *Pnoc* gene were obtained. RecA-mediated homologous recombination (58) was used to introduce eGFP into the *Pnoc* gene. The eGFP start codon was placed exactly into the position of the endogenous *Pnoc* start codon. To this end, 5´ and 3´ homology arms (0.7 and 1.5 kb long) flanking the start codon and exon 2 of *Pnoc*, respectively, were generated by PCR. After two rounds of homologous recombination, BAC clones containing the desired recombination were identified by Southern blot analysis. Sizing of the modified BACs revealed that BAC 452H11 contained > 120 kb sequence upstream of eGFP. This clone was chosen for pronucleus injection. Purified linearized BAC DNA was injected into the male pronuclei of fertilized FVB oocytes. Two lines of mice were obtained showing germline transmission. For details on the preparation of DNA and injection procedure see (59).

Mice were bred on a C57Bl/6J background and maintained on a 12 h light/dark cycle with free access to water and standard mouse chow (4.25% fat, RM3, Special Diet Services). Mice were housed in specific-pathogen free barrier facilities in individually-ventilated cages of mixed genotypes. Male transgenic mice were age-matched (3-5 months) and studied with

littermate controls. Experiments and findings described in this paper were designed and reported following the Animal Research: Reporting of In Vivo Experiments (ARRIVE) guidelines of animal experiment reporting (60). Where possible, investigators were blinded to the genotype of the study animals. Mice were randomized by genotype to study groups or a crossover design was used where indicated and study cohorts were matched for initial bodyweight where appropriate. Mice were group housed (3-5 per cage) unless stated.

Genotyping

Generic Cre-recombinase (5'-AGCGATGGATTTCCGTCTCT and 5'-CACCAGCTTGCATGATCTCC) and GFP (5'-AGCTAGCCACCATGGTGAGCAAGGGCGAGGAG and 5'-ATCTCGAGCTTGTACAGCTCGTCCATGCCG) primers were used to genotype *Agrp*-Cre, Vgat-Cre, *Pdyn*-Cre, Sf1-Cre, *Pnoc*-eGFP and *Pomc*-GFP mice. *Npy*-hrGFP mice were genotyped using the following primers 5'-TATGTGGACGGGGCAGAAGATCCAGG, 5'-CCCAGCTCACATATTTATCTAGAG and 5'-GGTGCGGTTGCCGTACTGGA.

Plasmids and Viruses

A cre-dependent ChR2-mCherry plasmid (pAAV-EF1a-double floxed-hChR2(H134R)-mCherry, Addgene plasmid #20297) and a flp-dependent ChR2-EYFP plasmid (pAAV-Ef1a-fDIO hChR2(H134R)-EYFP, Addgene #55639) were gifts from K. Deisseroth (61). hChR2(H134R)-mCherry was sub-cloned into the pAAV-Ef1a-fDIO hChR2(H134R)-EYFP vector using AscI and NheI restrictions sites to replace hChR2(H134R)-EYFP to make pAAV-Ef1a-fDIO hChR2(H134R)-mCherry. The sequence for jRGECO1a (pGP-CMV-NES-jRGECO1a; Addgene plasmid #61563) was a gift from D. Kim and GENIE project (41), the sequence for the hemagglutinin (HA)-tagged ribosomal protein (RiboTag) was provided by S. McKnight (36, 37). Sequences were then synthesized by GeneArt (Life Technologies) and sub-cloned into the pAAV-EF1a-double floxed-hChR2(H134R)-mCherry vector using AscI and NheI restriction sites

to invert the sequence and replace ChR2-mCherry. An ires-mCherry sequence was also inserted upstream of the RiboTag sequence to make the resulting plasmids, pAAV-EF1a-double floxed jRGECO1a and pAAV-EF1a- double floxed RiboTag-ires-mCherry. Plasmids for N-CretrcintG (pAAV-EF1a-N-CretrcintG, Addgene plasmid #69570), C-CreintG (pAAV-EF1a-C-CreintG, Addgene plasmid #69571) and DOG-flpo (pAAV-EF1a-Flp-DOG-NW, Addgene plasmid #75469) were gifts from C. Cepko (34, 62). Cre-dependent caspase-3 (pAAV-flex-taCasp3-TEVp; Addgene plasmid #45580) was a gift from N Shah (42). Viral plasmids were commercially packaged at Vector Biolabs (PA, USA) using the AAV1 or AAV2(retro) serotypes (44). Viral particles expressing cre-dependent YFP (pAAV-EF1a-DIO EYFP, Addgene plasmid #27056-AV1) were a gift from K. Deisseroth. AAV8 serotyped AAV particles expressing cre-dependent GFP tagged type-2 avian retroviral receptor (pAAV-EF1a-flex-GT, Addgene plasmid #26198) was a gift from E Callaway. Nuclear-tagged N2c-glycoprotein (pAAV-hSyn-flex H2B-EGFP-P2A-N2cG, Addgene plasmid #126469) and synaptophysin-mCherry (pAAV-hSyn-flex synaptophysin mCherry) were serotyped with AAV1 and a glycoprotein deficient rabies virus (CVS-N2c$^{\Delta G}$-mCherry, Addgene plasmid #126468) (43), pseudotyped with EnvA, were gifts from M. Strom and T. Margrie.

Stereotactic surgery

Age-matched (3-5 month) mice were placed in a KOPF stereotaxic frame and AAV particles or rabies virus were injected bilaterally (or unilaterally where stated) with a Hamilton syringe (0.3 μl/min, 0.15-0.3 μl per injection site) into either the aBNST (from bregma; anterior-posterior (AP), +0.30 mm; medial-lateral (ML), ±0.65 mm and dorsal-ventral from skull (DV), -4.30 and -4.50 mm), septum (AP, +0.30 mm; ML, ±0.65 mm; DV, -3.00 and -3.20 mm), arcuate nucleus (AP, -1.30 mm; ML, ±0.40 mm; DV, -5.80 and -6.10 mm) or VMH (AP, -1.35 mm; ML, ±0.45 mm; DV, -5.70 and -6.00 mm). In optogenetic and photometry studies, ferrule-attached

multimodal optical fibers (200 μm) were inserted bilaterally or unilaterally at a 10^{o} angle into (AP, -1.30 mm; ML, ±1.31 mm; DV, -6.30 mm) or dorsal (AP, -1.30 mm; ML, ±1.15 mm; DV, -5.40 mm) to the arcuate nucleus, or at a 5^{o} angle into the medial-dorsal region of the aBNST (AP, +0.30 mm; ML, ±1.15 mm; DV, -4.20 mm). Optical fiber tracts and viral expression was used to confirm correct stereotaxic placement in all mice post-mortem.

Optogenetics

Cre-dependent ChR2-mCherry (1.7 x 10^{13} GC/ml) or YFP (1.2 x 10^{13} GC/ml) AAVs were injected into the aBNST. *Pnoc*-eGFP mice were also injected with AAV1 particles containing N-CretrcintG (1.8 x10^{13} GC/ml) and C-CreintG (3.1 x10^{13} GC/ml). Flp-dependent ChR2-mCherry (2.0 x 10^{13} GC/ml) and DOG-flpo (1.8 x 10^{13} GC/ml) AAVs were also unilaterally injected into the aBNST. Ferrule-attached optical fiber implants were coupled to a ferrule-attached optical fiber (200 μm diameter, multimodal) connected to a collimated rotary joint (Doric Lenses), as described previously (63). The rotary joint was connected via an optical fiber to a 473 nm laser (Vortran). To control the pattern of laser stimulation, a STG pulse generator (Multichannel Systems) was used to send 5 ms digital pulses (10 Hz for 3 s, repeated every 4 s) to the laser interlock function. Laser output at the end of the implanted ferrules ranged between 10 and 12 mW.

Feeding behavior

4-month old male Vgat-Cre, *Pnoc*-eGFP and wild-type mice expressing cre-dependent ChR2-mCherry or YFP were used to assess feeding. Mouse habituation commenced 2 weeks after stereotaxic surgery and consisted of daily handling, optical fiber tethering and mock overnight fasting in the home cage. On the day of the test, overnight fasted mice were tethered and placed in a clean home cage with free access to water. Laser stimulation began 10 minutes prior to the presentation of normal chow and continued for a further 4 hours. Food

consumption was assessed throughout the stimulation period and for a further 2 hours thereafter. Stimulated and non-stimulated mice were crossed over the following week.

Anxiety behavior

Wild-type littermates and *Pnoc*-eGFP mice expressing cre-recombinase with and without ChR2-mCherry in the aBNST were used to assess anxiety-related behavior. Mouse habituation commenced 2 weeks after stereotaxic surgery and consisted of daily handling and optical fiber tethering. Mice were transferred to a novel room, tethered to a laser attached optical fiber and placed in a novel open-field arena (0.45 m open-top, square wooden box). A burst pattern (10 Hz for 3 s, repeated every 4 s) of laser stimulation was then immediately initiated and mouse locomotion was video recorded and tracked using Ethovision (Noldus) software for 30 minutes. A week later, mice were tested on an elevated-O-maze (Panlabs) during continuous (burst) laser stimulation for 10 minutes. Video tracking and manual scoring were used to determine the time spent and entries into the anxiogenic open zones.

Fiber Photometry

Fiber photometry was performed on 4-month old male *Pnoc*-eGFP mice injected with AAV particles containing N-CretrcintG (1.8 $x10^{13}$ GC/ml), C-CreintG (3.1 $x10^{13}$ GC/ml) and cre-dependent jRGECO1a ($0.9x10^{13}$ GC/ml) in the aBNST. In some studies, the arcuate nucleus was injected with jRGECO1a ($0.9x10^{13}$ GC/ml) in *Agrp*-Cre mice. Implanted optical fibers were coupled to a ferrule-attached optical fiber (200 μm diameter, multimodal) connected to a fiberoptometer (NPI electronic, Germany). Briefly, light from a 565 nm light-emitting diode (LED) was passed through a 545 ± 15 nm excitation filter and down the optical fiber via a dichroic mirror (transmission ≥570 nm). jRGECO1a florescence (peak ~600 nm) was transmitted back through the dichroic mirror, a 620 ± 30 nm emission filter and into a photomultiplier. Voltage output was low-pass filtered at 340 Hz and sampled at 200 Hz using

PClamp10 software. Continuous low power (100-120 μW at fiber tip) light was used to excite jRGECO1a. Any ambient and LED light that may have been captured by the photomultiplier was subtracted from florescence by generating templates acquired in between trials but recorded without attaching the optical fiber to the implanted ferrules. During photometry, mice were video recorded and tracked with Ethovision software which was digitally coupled to the fiberoptometer to time-lock the behavior with florescence output.

Mouse habituation commenced 2 weeks after surgery and comprised of daily handling, optical fiber tethering and exploration of an open-field arena (0.45 m open-top, square wooden box) with 2 circular pots (5 cm diameter) centered in the middle containing normal chow or a familiar object (chew block). A mock overnight fast was conducted in the home cage and in the open-field arena on consecutive weeks. A week later, overnight fasted mice were tethered and placed in the arena containing 2 pots without food. After 10 minutes of arena habituation, the LED light was turned on and recordings commenced. After 10 minutes a novel object (metal nut) was added to one pot and then after another 10 minutes a food pellet (normal chow, ~1 cm^3) was added to the remaining pot. Recordings were continued for a further 10 minutes. Voltages were aligned to the time in which the mice approached the novel object or the first bite of food. For studies investigating the effects of optogenetic activation of aBNST nociceptin neurons on AgRP neuronal activity, after a 10-minute control period, the aBNST was photostimulated for 2 minutes during continuous excitation and recording of jRGECO1a activity in the arcuate nucleus. The change in fluorescence (ΔF) at each data point was divided by the median fluorescence (F) during baseline recordings (0.5-2 minutes before the behavioral event). Sample rate was then reduced to 1 Hz by IgorPro6 software for statistical purposes.

Caspase induced-cell death

Caspase-induced cell death was performed using 5-month old male *Pnoc*-eGFP mice and wild-type littermate controls injected with AAV particles containing N-CretrcintG (1.1 x 10^{13} GC/ml), C-CreintG (1.9 x 10^{13} GC/ml), cre-dependent ChR2-mCherry (1.2 x 10^{13} GC/ml) with or without cre-dependent caspase-3 (1.1 x 10^{12} GC/ml) into the aBNST. Mice were group housed and weighed weekly before and after stereotaxic surgery. Whole-body fat and lean mass were measured 6 weeks after surgery by EchoMRI. Mice were also singly housed 4-weeks post-surgery for at least 2 weeks before measurements of ad-libitum food intake, as described previously (63). Post-mortem PFA-fixed 35 μm coronal slices containing the aBNST were used to count mCherry positive somas in mice expressing ChR2-mCherry with or without caspase-3.

RiboTag and RNA sequencing

The RiboTag approach was performed as described previously (36, 37). AAV1 particles containing N-CretrcintG (1.8 x 10^{13} GC/ml), C-CreintG (3.1 x 10^{13} GC/ml) and cre-dependent RiboTag-ires-mCherry (0.8 x 10^{13} GC/ml) were bilaterally injected into the aBNST of 4-month old male *Pnoc*-eGFP mice. 4 weeks after surgery, mice were culled and the aBNST was dissected and homogenized in 800 μl of polysome buffer (50 mM Tris, pH 7.5, 100 mM KCl, 12 mM $MgCl_2$, 1 % v/v IGEPAL, 1 mM DTT, 200 U/ml RNasin (Promega), 1 mg/ml heparin, 100 μg/ml cycloheximide (Sigma-Aldrich), protease inhibitor cocktail (GE Healthcare). Homogenates were centrifuged at 10,000 x g for 10 min at 4 ^{o}C to create a post-mitochondrial supernatant. 40 μl of supernatant was set aside to extract total aBNST RNA. 750 μl of the remaining supernatant was incubated overnight at 4 ^{o}C with anti-HA coupled protein G beads. Magnetically captured beads were washed in high salt buffer (50 mM Tris, pH 7.5, 300 mM KCl, 12 mM $MgCl_2$, 1 % v/v IGEPAL, 1 mM DTT, 100 μg/ml cycloheximide) and polysomes eluted with lysis buffer (Qiagen, Cat. 74106). RNA was extracted from the eluted samples and

homogenate supernatant using an RNeasy Mini Kit (Qiagen, Cat. 74106). RNA was DNAase treated (Qiagen, Cat. 79254). 20 ng of total RNA was ribosomal RNA depleted using a NEBNext rRNA depletion kit (NEB #E6310) and RNA libraries were prepared using NEBNext Ultra II directional RNA library prep kit for Illumina (NEB #E7760) and PCR enrichment performed with NEBNext multiplex oligos for Illumina set 1 (NEB #E7335). Paired end, 100 base-pair sequences were obtained using a HiSeq 2500 (v4 reagents) kit. Raw RNA-sequencing reads were mapped with STAR aligner (version 020201) against Ensembl mouse genome reference sequence assembly (mm10) and gencode vM19 gene annotations (64). Differential expression analysis was performed on the counts data using DESeq2 bioconductor package (version 1.22.2). DESeq2 package uses negative binomial model to model read counts and then performs statistical tests for differential expression of genes (65). Raw p values were adjusted for multiple testing with the Benjamini-Hochberg procedure. Data is deposited on Gene Expression Omnibus (https://www.ncbi.nlm.nih.gov/geo), accession number GSE135982.

Ex vivo electrophysiology and imaging

AAV particles containing cre-dependent ChR2-mCherry (1.7 x 10^{13} GC/ml) or jRGECO1a (0.9x10^{13} GC/ml) with or without N-CretrcintG (1.8 x10^{13} GC/ml) and C-CreintG (3.1 x10^{13} GC/ml) were injected into transgenic mice expressing Vgat-Cre, *Pdyn*-Cre, Sf1-Cre, or *Pnoc*-eGFP mice crossed with either *Pomc*-GFP or *Npy*-hrGFP mice. Ex vivo slices were maintained at room temperature (22-25°C) in an external solution containing (in mM) NaCl 125, KCl 2.5, NaH_2PO_4 1.25, $NaHCO_3$ 25, $CaCl_2$ 2, $MgCl_2$ 1, D-glucose 10, D-mannitol 15, equilibrated with 95% O_2, 5% CO_2, pH 7.4. Whole-cell current-clamp recordings were made using borosilicate glass pipettes (4-8 MΩ) containing (in mM) Kgluconate 130, KCl 10, EGTA 0.5, NaCl 1, $CaCl_2$ 0.28, $MgCl_2$ 3, Na_2ATP 3, GTP 0.3, phosphocreatine 14 and HEPES 10 (pH 7.2). Nociceptin

(Tocris) was bath applied and input resistance monitored by periodic hyperpolarizing current pulses. Synaptic release from ChR2-expressing axonal terminals was evoked by pulses (4 ms) of light (488 nm) generated by a monochromator (Polychrome V). A burst stimulating protocol (10 Hz for 3 s and repeated every 4 s) was used to assess changes in spontaneous action potential firing frequency. jRGECO1a florescence was excited by 50 ms pulses of 590 nm light at 0.5 Hz using a monochromator. Depolarizing current injections were used to evoke action potential firing while simultaneously recording florescence intensity.

Whole-cell voltage-clamp recordings were made at -70 mV in a modified internal solution with Kgluconate replaced with CsCl (130 mM), where excitatory and inhibitory synaptic currents are observed as inward currents. Synaptic currents were photostimulated (4 ms pulse of 488 nm light) at 0.5 Hz. Bath application of 20 μM (+)-bicuculline or 5 μM 2,3-dihydroxy-6-nitro-7-sulfamoyl-benzo(f)quinoxaline-2,3-dione (NBQX) with 50 μM D-2-amino-5-phosphonopentanoate (D-AP5) were used to distinguish GABAergic or glutamatergic events, respectively.

Imaging, immunohistochemistry and in situ hybridization

Mice were perfused with paraformaldehyde (4% w/v) and frozen coronal sections (30-35 μm) were cut, as previously described (66). aBNST sections were incubated with rabbit anti-nociceptin (1:500; Abcam, Cat. ab10277) and detection performed using a secondary antibody coupled to Alexa-Fluor-594 (1:200, Invitrogen, Cat. A21442). Florescence images were captured using an Olympus IX70 microscope. In situ hybridization on mouse brain slices were performed using Digoxigenin labelled *Pnoc* antisense mRNA (mRNA 1-932; NM_010932).

Statistics

Statistical significance was calculated using repeated measures (RM) two-way ANOVA followed by Sidak post-hoc analysis or Student's two-tailed paired, unpaired and one-sample t-test, where stated. Data are expressed as mean ± standard error of mean (SEM). A p value less than 0.05 was considered significant.

Study approval

All animal studies were performed in accordance to the United Kingdom Animals (Scientific Procedures) Act (1986), amended regulations (2012), and approved by Imperial College Animal Welfare and Ethical Review Body.

Author contributions

M.A.S., A.I.C., J.A.G., P.V., E.E.I. and P.C. performed experiments. H.U.Z. contributed reagents. M.A.S. and S.K. analyzed data. M.A.S. and D.J.W. developed the concepts, supervised the work and wrote the manuscript. D.J.W. secured funding. All authors contributed to the editing of the manuscript.

Acknowledgements

We thank the following for their helpful advice and reagents: Connie Cepko and Jonathan Tang (Harvard University), Stanley McKnight (University of Washington), Troy Margrie and Molly Strom (University College London). This work was funded by the Medical Research Council (MC-A654-5QB40) to D.J.W.

References

1. Andermann ML, and Lowell BB. Toward a Wiring Diagram Understanding of Appetite Control. *Neuron.* 2017;95(4):757-778.
2. Denis RG, et al. Palatability Can Drive Feeding Independent of AgRP Neurons. *Cell Metab.* 2015;22(4):646-657.
3. Sternson SM, Nicholas Betley J, and Cao ZF. Neural circuits and motivational processes for hunger. *Curr Opin Neurobiol.* 2013;23(3):353-360.
4. Aponte Y, Atasoy D, and Sternson SM. AGRP neurons are sufficient to orchestrate feeding behavior rapidly and without training. *Nat Neurosci.* 2011;14(3):351-355.
5. Krashes MJ, et al. Rapid, reversible activation of AgRP neurons drives feeding behavior in mice. *J Clin Invest.* 2011;121(4):1424-1428.
6. Burnett CJ, et al. Hunger-Driven Motivational State Competition. *Neuron.* 2016;92(1):187-201.
7. Garfield AS, et al. Dynamic GABAergic afferent modulation of AgRP neurons. *Nat Neurosci.* 2016;19(12):1628-1635.
8. Krashes MJ, et al. An excitatory paraventricular nucleus to AgRP neuron circuit that drives hunger. *Nature.* 2014;507(7491):238-242.
9. Betley JN, et al. Neurons for hunger and thirst transmit a negative-valence teaching signal. *Nature.* 2015;521(7551):180-185.
10. Beutler LR, et al. Dynamics of Gut-Brain Communication Underlying Hunger. *Neuron.* 2017;96(2):461-475 e5.
11. Chen Y, Lin YC, Kuo TW, and Knight ZA. Sensory detection of food rapidly modulates arcuate feeding circuits. *Cell.* 2015;160(5):829-841.
12. Mandelblat-Cerf Y, et al. Arcuate hypothalamic AgRP and putative POMC neurons show opposite changes in spiking across multiple timescales. *Elife.* 2015;4:e07122.
13. Su Z, Alhadeff AL, and Betley JN. Nutritive, Post-ingestive Signals Are the Primary Regulators of AgRP Neuron Activity. *Cell Rep.* 2017;21(10):2724-2736.
14. Chen Y, Lin YC, Zimmerman CA, Essner RA, and Knight ZA. Hunger neurons drive feeding through a sustained, positive reinforcement signal. *Elife.* 2016;5:e18640.
15. Wang D, et al. Whole-brain mapping of the direct inputs and axonal projections of POMC and AgRP neurons. *Front Neuroanat.* 2015;9:40.
16. Dong HW, and Swanson LW. Projections from bed nuclei of the stria terminalis, anteromedial area: cerebral hemisphere integration of neuroendocrine, autonomic, and behavioral aspects of energy balance. *J Comp Neurol.* 2006;494(1):142-178.
17. Betley JN, Cao ZF, Ritola KD, and Sternson SM. Parallel, redundant circuit organization for homeostatic control of feeding behavior. *Cell.* 2013;155(6):1337-1350.
18. Jennings JH, Rizzi G, Stamatakis AM, Ung RL, and Stuber GD. The inhibitory circuit architecture of the lateral hypothalamus orchestrates feeding. *Science.* 2013;341(6153):1517-1521.
19. Rollins BL, Stines SG, and King BM. Role of the stria terminalis in food intake and body weight in rats. *Physiol Behav.* 2006;89(2):139-145.
20. Kash TL, et al. Neuropeptide regulation of signaling and behavior in the BNST. *Mol Cells.* 2015;38(1):1-13.
21. Ch'ng S, Fu J, Brown RM, McDougall SJ, and Lawrence AJ. The intersection of stress and reward: BNST modulation of aversive and appetitive states. *Prog Neuropsychopharmacol Biol Psychiatry.* 2018;87(Pt A):108-125.

22. Gungor NZ, and Pare D. Functional Heterogeneity in the Bed Nucleus of the Stria Terminalis. *J Neurosci.* 2016;36(31):8038-8049.
23. Giardino WJ, et al. Parallel circuits from the bed nuclei of stria terminalis to the lateral hypothalamus drive opposing emotional states. *Nat Neurosci.* 2018;21(8):1084-1095.
24. Zhang X, and van den Pol AN. Direct inhibition of arcuate proopiomelanocortin neurons: a potential mechanism for the orexigenic actions of dynorphin. *J Physiol.* 2013;591(7):1731-1747.
25. Bewick GA, et al. Hypothalamic cocaine- and amphetamine-regulated transcript (CART) and agouti-related protein (AgRP) neurons coexpress the NOP1 receptor and nociceptin alters CART and AgRP release. *Endocrinology.* 2005;146(8):3526-3534.
26. Wagner EJ, Ronnekleiv OK, Grandy DK, and Kelly MJ. The peptide orphanin FQ inhibits beta-endorphin neurons and neurosecretory cells in the hypothalamic arcuate nucleus by activating an inwardly-rectifying K+ conductance. *Neuroendocrinology.* 1998;67(2):73-82.
27. Li C, et al. Presynaptic inhibition of gamma-aminobutyric acid release in the bed nucleus of the stria terminalis by kappa opioid receptor signaling. *Biol Psychiatry.* 2012;71(8):725-732.
28. Hernandez J, et al. Nociceptin/orphanin FQ modulates energy homeostasis through inhibition of neurotransmission at VMN SF-1/ARC POMC synapses in a sex- and diet-dependent manner. *Biol Sex Differ.* 2019;10(1):9.
29. Chee MJ, Price CJ, Statnick MA, and Colmers WF. Nociceptin/orphanin FQ suppresses the excitability of neurons in the ventromedial nucleus of the hypothalamus. *J Physiol.* 2011;589(Pt 13):3103-3114.
30. Lein ES, et al. Genome-wide atlas of gene expression in the adult mouse brain. *Nature.* 2007;445(7124):168-176.
31. Boom A, et al. Distribution of the nociceptin and nocistatin precursor transcript in the mouse central nervous system. *Neuroscience.* 1999;91(3):991-1007.
32. Ikeda K, et al. Distribution of prepro-nociceptin/orphanin FQ mRNA and its receptor mRNA in developing and adult mouse central nervous systems. *J Comp Neurol.* 1998;399(1):139-151.
33. Neal CR, Jr., et al. Localization of orphanin FQ (nociceptin) peptide and messenger RNA in the central nervous system of the rat. *J Comp Neurol.* 1999;406(4):503-547.
34. Tang JC, et al. Cell type-specific manipulation with GFP-dependent Cre recombinase. *Nat Neurosci.* 2015;18(9):1334-1341.
35. Tang JC, et al. A nanobody-based system using fluorescent proteins as scaffolds for cell-specific gene manipulation. *Cell.* 2013;154(4):928-939.
36. Sanz E, et al. Cell-type-specific isolation of ribosome-associated mRNA from complex tissues. *Proc Natl Acad Sci U S A.* 2009;106(33):13939-13944.
37. Sanz E, et al. Fertility-regulating Kiss1 neurons arise from hypothalamic POMC-expressing progenitors. *J Neurosci.* 2015;35(14):5549-5556.
38. Sweeney P, Li C, and Yang Y. Appetite suppressive role of medial septal glutamatergic neurons. *Proc Natl Acad Sci U S A.* 2017;114(52):13816-13821.
39. Sweeney P, and Yang Y. An excitatory ventral hippocampus to lateral septum circuit that suppresses feeding. *Nat Commun.* 2015;6:10188.
40. Sweeney P, and Yang Y. An Inhibitory Septum to Lateral Hypothalamus Circuit That Suppresses Feeding. *J Neurosci.* 2016;36(44):11185-11195.

41. Dana H, et al. Sensitive red protein calcium indicators for imaging neural activity. *Elife.* 2016;5:e12727.
42. Yang CF, et al. Sexually dimorphic neurons in the ventromedial hypothalamus govern mating in both sexes and aggression in males. *Cell.* 2013;153(4):896-909.
43. Reardon TR, et al. Rabies Virus CVS-N2c(DeltaG) Strain Enhances Retrograde Synaptic Transfer and Neuronal Viability. *Neuron.* 2016;89(4):711-724.
44. Tervo DG, et al. A Designer AAV Variant Permits Efficient Retrograde Access to Projection Neurons. *Neuron.* 2016;92(2):372-382.
45. Avery SN, et al. BNST neurocircuitry in humans. *Neuroimage.* 2014;91:311-323.
46. Dong HW, and Swanson LW. Organization of axonal projections from the anterolateral area of the bed nuclei of the stria terminalis. *J Comp Neurol.* 2004;468(2):277-298.
47. Lebow MA, and Chen A. Overshadowed by the amygdala: the bed nucleus of the stria terminalis emerges as key to psychiatric disorders. *Mol Psychiatry.* 2016;21(4):450-463.
48. McDonald AJ. Cortical pathways to the mammalian amygdala. *Prog Neurobiol.* 1998;55(3):257-332.
49. Vann SD, Aggleton JP, and Maguire EA. What does the retrosplenial cortex do? *Nat Rev Neurosci.* 2009;10(11):792-802.
50. Navarro M, et al. Lateral Hypothalamus GABAergic Neurons Modulate Consummatory Behaviors Regardless of the Caloric Content or Biological Relevance of the Consumed Stimuli. *Neuropsychopharmacology.* 2016;41(6):1505-1512.
51. Ciccocioppo R, et al. Reversal of stress- and CRF-induced anorexia in rats by the synthetic nociceptin/orphanin FQ receptor agonist, Ro 64-6198. *Psychopharmacology (Berl).* 2002;161(2):113-119.
52. Xu AW, et al. Effects of hypothalamic neurodegeneration on energy balance. *PLoS Biol.* 2005;3(12):e415.
53. Hardaway JA, et al. Central Amygdala Prepronociceptin-Expressing Neurons Mediate Palatable Food Consumption and Reward. *Neuron.* 2019;102:1037-1052.
54. Parker KE, et al. A Paranigral VTA Nociceptin Circuit that Constrains Motivation for Reward. *Cell.* 2019;178(3):653-671 e19.
55. Stephens MA, and Wand G. Stress and the HPA axis: role of glucocorticoids in alcohol dependence. *Alcohol Res.* 2012;34(4):468-483.
56. Stevens FL, Hurley RA, and Taber KH. Anterior cingulate cortex: unique role in cognition and emotion. *J Neuropsychiatry Clin Neurosci.* 2011;23(2):121-125.
57. Geliebter A, Benson L, Pantazatos SP, Hirsch J, and Carnell S. Greater anterior cingulate activation and connectivity in response to visual and auditory high-calorie food cues in binge eating: Preliminary findings. *Appetite.* 2016;96:195-202.
58. Yang XW, Model P, and Heintz N. Homologous recombination based modification in Escherichia coli and germline transmission in transgenic mice of a bacterial artificial chromosome. *Nat Biotechnol.* 1997;15(9):859-865.
59. Zeilhofer HU, et al. Glycinergic neurons expressing enhanced green fluorescent protein in bacterial artificial chromosome transgenic mice. *J Comp Neurol.* 2005;482(2):123-141.
60. Kilkenny C, Browne WJ, Cuthill IC, Emerson M, and Altman DG. Improving bioscience research reporting: the ARRIVE guidelines for reporting animal research. *PLoS Biol.* 2010;8(6):e1000412.

61. Fenno LE, et al. Targeting cells with single vectors using multiple-feature Boolean logic. *Nat Methods.* 2014;11(7):763-772.
62. Tang JC, et al. Detection and manipulation of live antigen-expressing cells using conditionally stable nanobodies. *Elife.* 2016;5:e15312.
63. Viskaitis P, et al. Modulation of SF1 Neuron Activity Coordinately Regulates Both Feeding Behavior and Associated Emotional States. *Cell Rep.* 2017;21(12):3559-3572.
64. Dobin A, et al. STAR: ultrafast universal RNA-seq aligner. *Bioinformatics.* 2013;29(1):15-21.
65. Love MI, Huber W, and Anders S. Moderated estimation of fold change and dispersion for RNA-seq data with DESeq2. *Genome Biol.* 2014;15(12):550.
66. Choudhury AI, et al. The role of insulin receptor substrate 2 in hypothalamic and beta cell function. *J Clin Invest.* 2005;115(4):940-950.

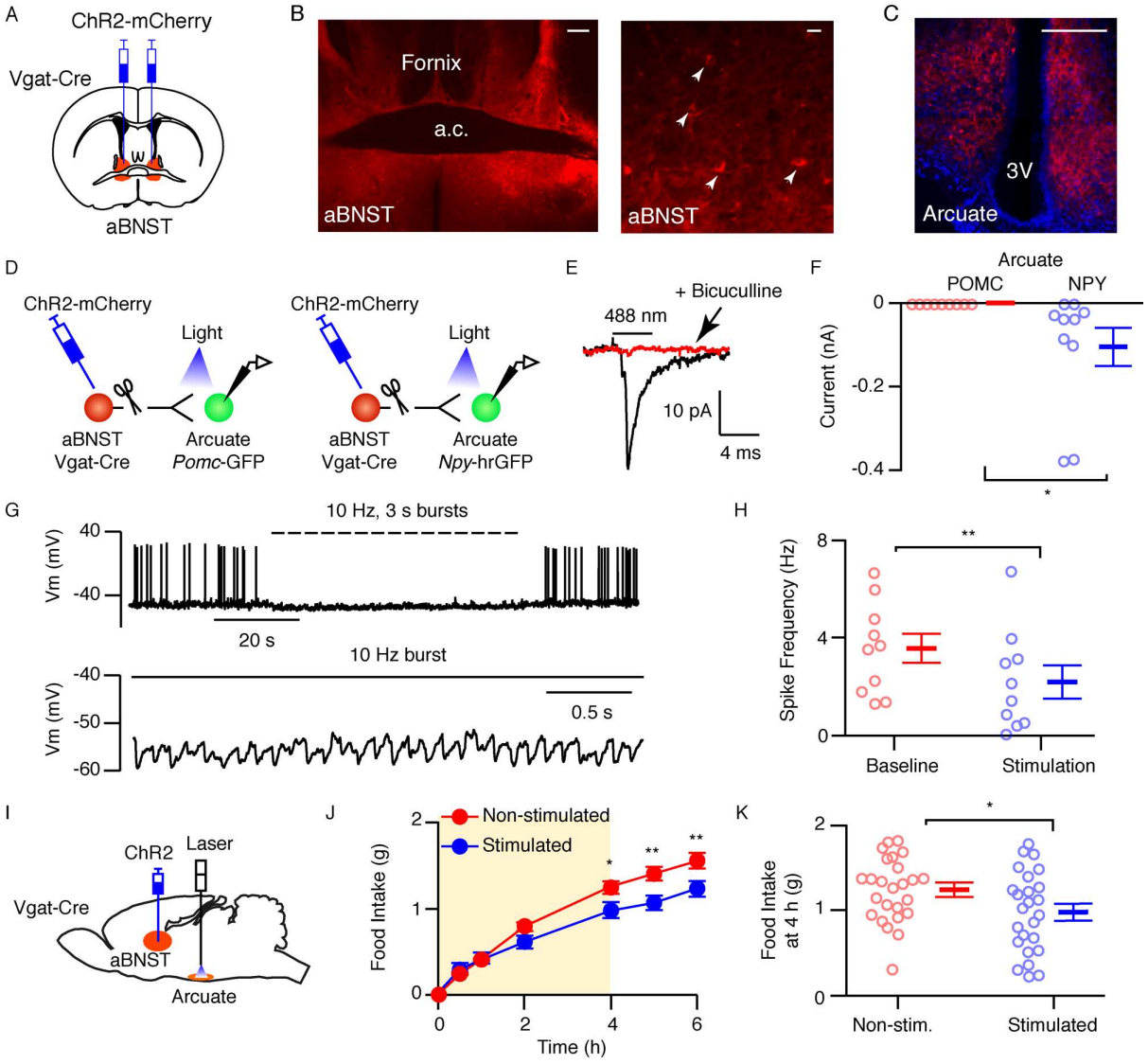

Figure 1. Photostimulation of aBNST GABAergic axons in the arcuate nucleus suppresses feeding.

(**A**) aBNST (red) with ChR2-mCherry injections. (**B**) Mosaic images (n = 35) of aBNST (expanded right) and arcuate nucleus (**C**) from Vgat-Cre mice with ChR2-mCherry AAV injected into the aBNST. Scale bars are 200 μm for low and 20 μm for high magnification images. 3V, 3rd ventricle; a.c., anterior commissure. (**D**) Diagram of Vgat-Cre crossed with *Pomc*-GFP (left) or *Npy*-hrGFP (right) mice with ChR2-mCherry in the aBNST. (**E**) Photostimulated synaptic currents from an arcuate NPY neuron in the absence (black) and presence of 20 μM (+)-bicuculline (red, n = 10). (**F**) Synaptic currents in arcuate POMC (n = 9 neurons from 3 mice)

and NPY (n = 10 neurons from 3 mice) neurons. Mean ± SEM, * $p<0.05$ (unpaired t-test, $t(17) = 2.15$, $p = 0.046$). (**G**) Voltage traces (expanded below) from NPY neuron during photostimulation of aBNST axons (n = 10). (**H**) Action potential frequency in NPY neurons (n = 10 neurons from 3 mice) before (baseline) and during photostimulation of aBNST axons. Mean ± SEM, ** $p<0.01$ (paired t-test, $t(9) = 3.33$, $p = 0.009$). (**I**) aBNST with ChR2-mCherry injections and optical fiber implants in the arcuate nucleus. (**J**) Cumulative food intake in fasted Vgat-Cre mice during (shaded area) and after photostimulation of ChR2-mCherry expressing axons from the aBNST. Food intake was measured in mice without (red) and with photostimulation (blue). Mean ± SEM, n = 25 mice. 2-way RM ANOVA (Interaction: $f(6,288) = 9.58$, $p < 0.0001$; stimulation: $f(1,48) = 3.68$, $p = 0.06$), Sidak post-hoc test, * $p<0.05$, ** $p<0.01$. (**K**) Food intake at 4 h from non-stimulated (non-stim.) and stimulated mice. Mean ± SEM, n = 25 mice. * $p<0.05$ (paired t-test, $t(24) = 2.46$, $p = 0.021$).

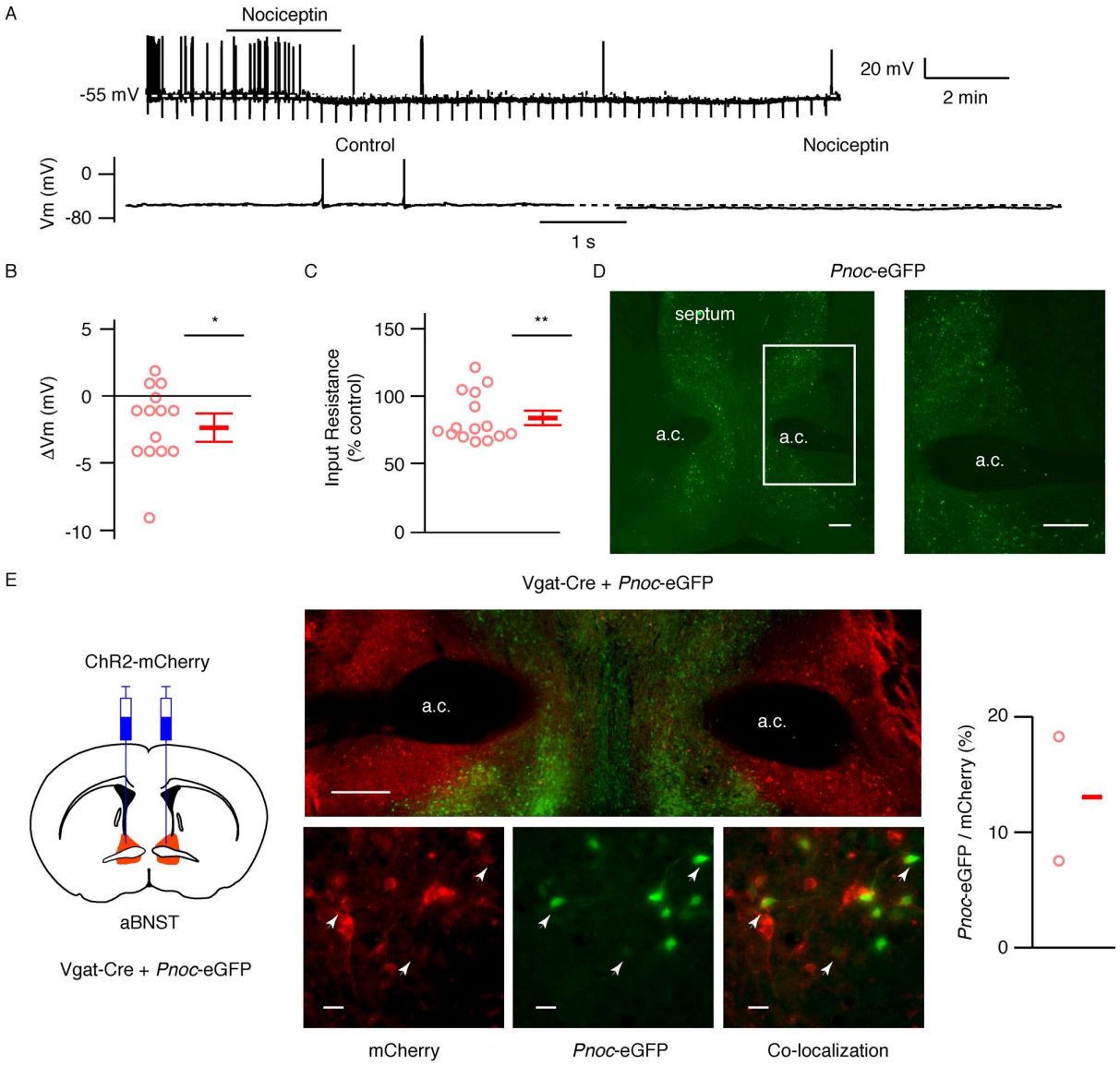

Figure 2. Nociceptin is expressed in a subpopulation of Vgat neurons.

(**A**) Voltage traces (expanded below) from a NPY neuron during 0.5 μM nociceptin application, where indicated (n = 15). (**B** and **C**) Nociceptin-induced change in membrane potential (Vm, **B**) and input resistance (**C**) in NPY neurons. Mean ± SEM, n = 15 neurons from 8 mice, * $p<0.05$ (Vm: one-sampled t-test, $t(14) = 2.88$, $p = 0.012$), ** $p<0.01$ (input resistance: one-sampled t-test, $t(14) = 4.05$, $p = 0.0012$). (**D**) Image of a coronal section (expanded right) containing eGFP-expressing neurons driven by the *Pnoc* promoter (n = 10). a.c., anterior commissure. Scale bars are 200 μm. (**E**) Diagram (left) of Vgat-Cre crossed with *Pnoc*-eGFP mice and injected with ChR2-mCherry AAV. Low magnification mosaic (top middle) and expanded

(bottom middle) images showing *Pnoc*-eGFP (green) expression in sub-population of Vgat-Cre neurons expressing ChR2-mCherry (red). Percentage of Vgat neurons expressing ChR2-mCherry that co-express *Pnoc*-eGFP (right). Mean from 2 mice (338 out of 1103 Vgat neurons co-expressed *Pnoc*-eGFP). Scale bars are 200 μm for low and 20 μm for high magnification images.

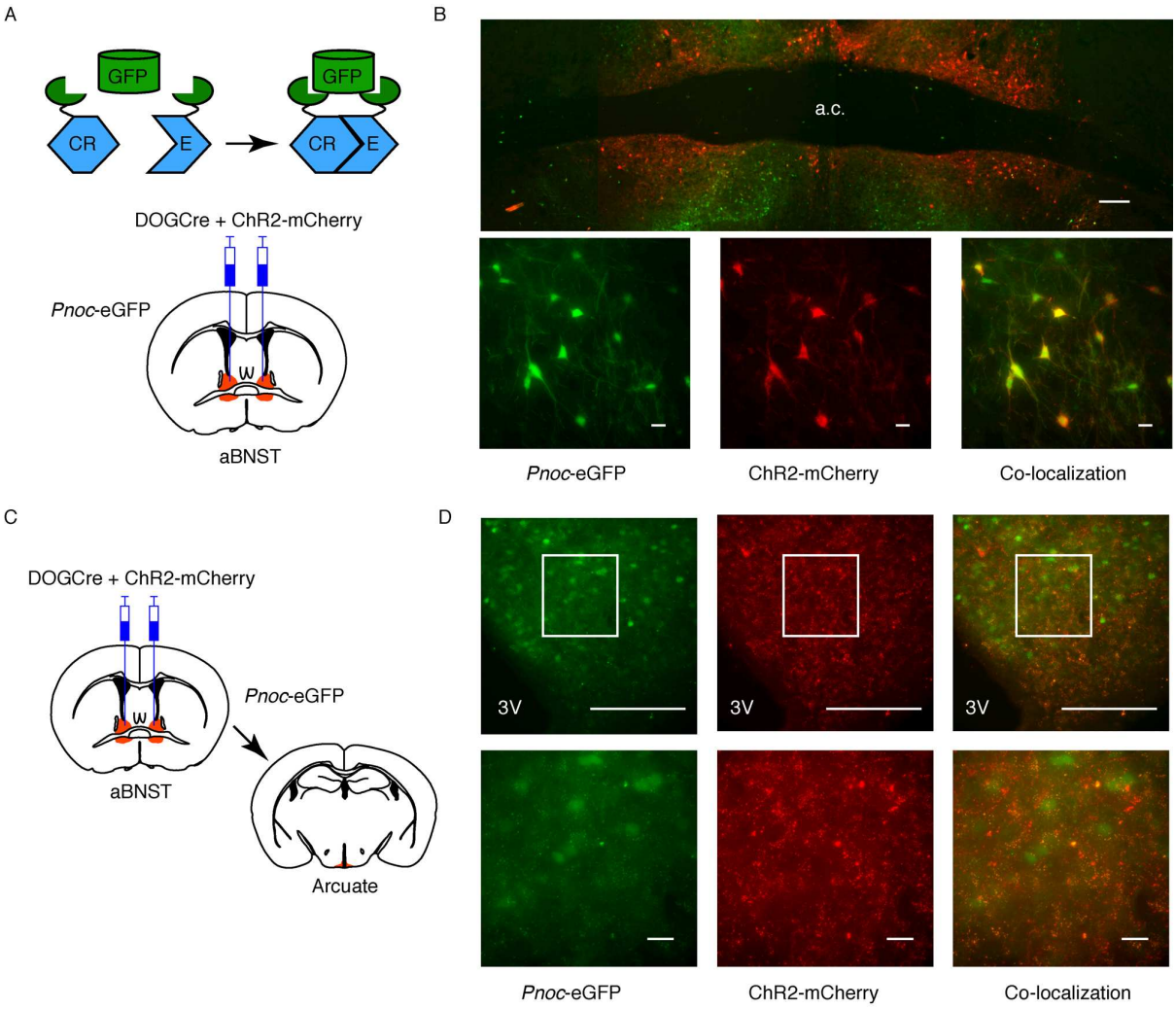

Figure 3. Nociceptin neurons project to the arcuate nucleus.

(**A**) Diagrams of 'Dependent-On-GFP' (DOGCre) technology used to express cre-recombinase in *Pnoc*-eGFP neurons (top) and injection of DOGCre (C-creintG and N-cretrcintG) and ChR2-mCherry AAVs into the aBNST (bottom). (**B**) Mosaic images (expanded below) showing the expression of *Pnoc*-eGFP (green) and ChR2-mCherry (red) in the aBNST (n = 47). (**C**) Diagrams showing the injection of DOGCre and ChR2-mCherry AAVs into the aBNST and corresponding arcuate nucleus section (right). (**D**) Coronal sections (expanded below) showing ChR2-mCherry expression in axons in the arcuate nucleus (red) and eGFP driven by *Pnoc* promoter (green, n = 10). Scale bars are 200 μm for low and 20 μm for high magnification images. 3V, 3rd ventricle; a.c., anterior commissure.

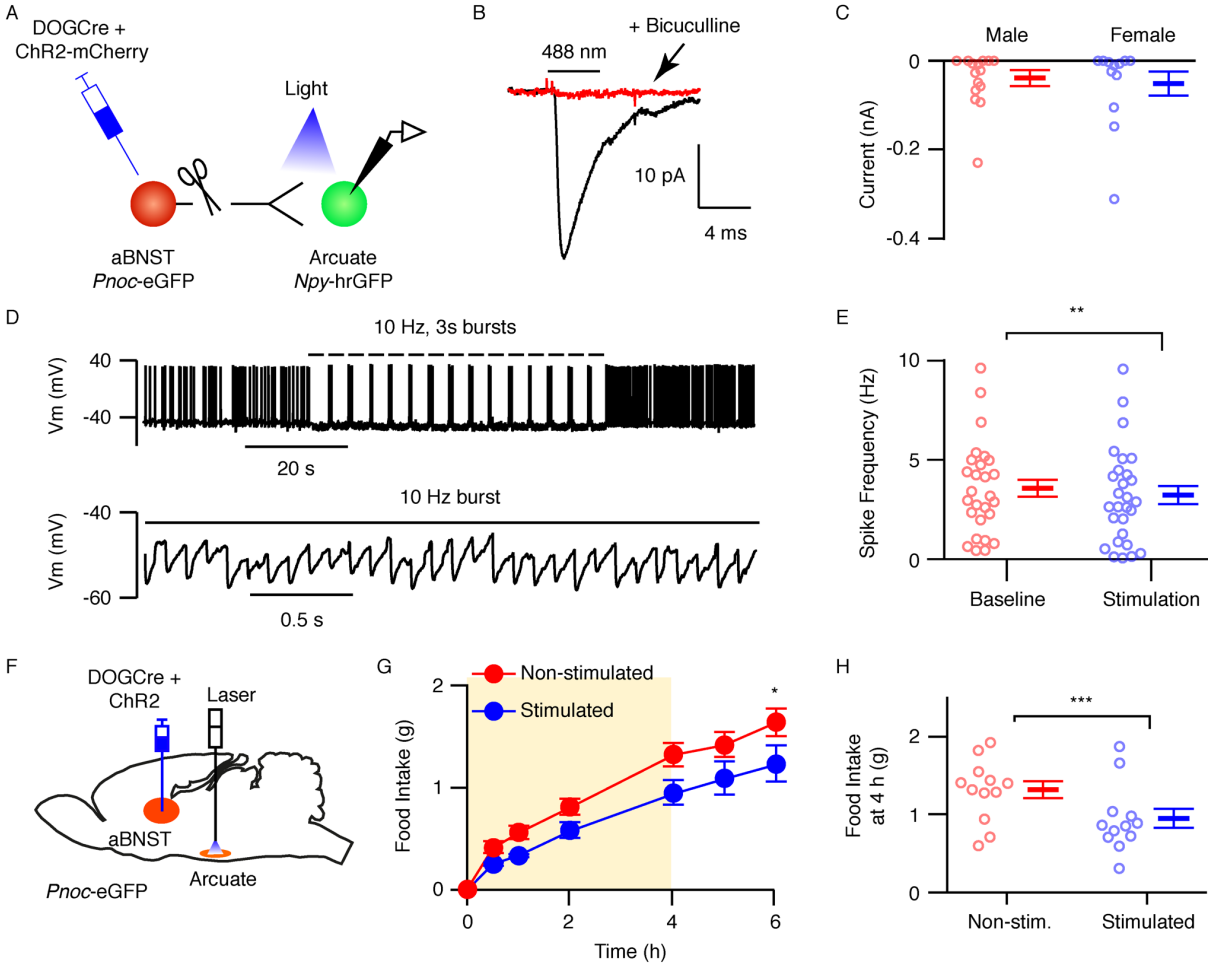

Figure 4. Photostimulation of aBNST nociceptin axons in the arcuate nucleus suppresses feeding.

(**A**) Diagram of *Pnoc*-eGFP mice crossed with *Npy*-hrGFP mice and injected with DOGCre and ChR2-mCherry AAVs into the aBNST. (**B**) Ensembled synaptic currents from an arcuate NPY neuron (n = 27) in the absence (black) and presence of 20 μM (+)-bicuculline (red). (**C**) Photostimulated synaptic currents in arcuate NPY neurons from male (n = 15 neurons from 5 mice) and female (n = 12 neurons from 3 mice) mice. Mean ± SEM, unpaired t-test between gender (t (25) = 0.35, p = 0.73). (**D**) Voltage traces (expanded below) from an arcuate NPY neuron during photostimulation (where indicated) of ChR2-mCherry expressing aBNST axons from *Pnoc*-eGFP mice (n = 28). (**E**) Arcuate NPY neuronal action potential frequency (n = 28

neurons from 9 mice) before (baseline) and during photostimulation of aBNST axons. Mean ± SEM, ** $p<0.01$ (paired t-test, $t(27) = 3.33$, $p = 0.003$). (**F**) Drawing of a sagittal section containing the aBNST with DOGCre and ChR2-mCherry AAV injections and optical fiber implants into the arcuate nucleus. (**G**) Cumulative food intake following an overnight fast in *Pnoc*-eGFP mice injected with DOGCre and ChR2-mCherry AAVs into the aBNST during (shaded area; 3 s 10 Hz bursts every 4 s) and after photostimulation of aBNST *Pnoc* fibers in the arcuate nucleus. Food intake was measured without (non-stimulated, red) and with photoexcitation (stimulated, blue). Mean ± SEM, n = 12 mice, 2-way RM ANOVA (Interaction: $f(6,132) = 2.15$, $p = 0.052$; stimulation: $f(1,22) = 4.76$, $p = 0.040$), Sidak post-hoc test, * $p<0.05$. (**H**) Food intake following the 4 h photostimulation period from non-stimulated (red, non-stim.) and stimulated (blue) mice. Mean ± SEM, n = 12 mice *** $p<0.001$ (paired t-test, $t(11) = 4.52$, $p = 0.0009$).

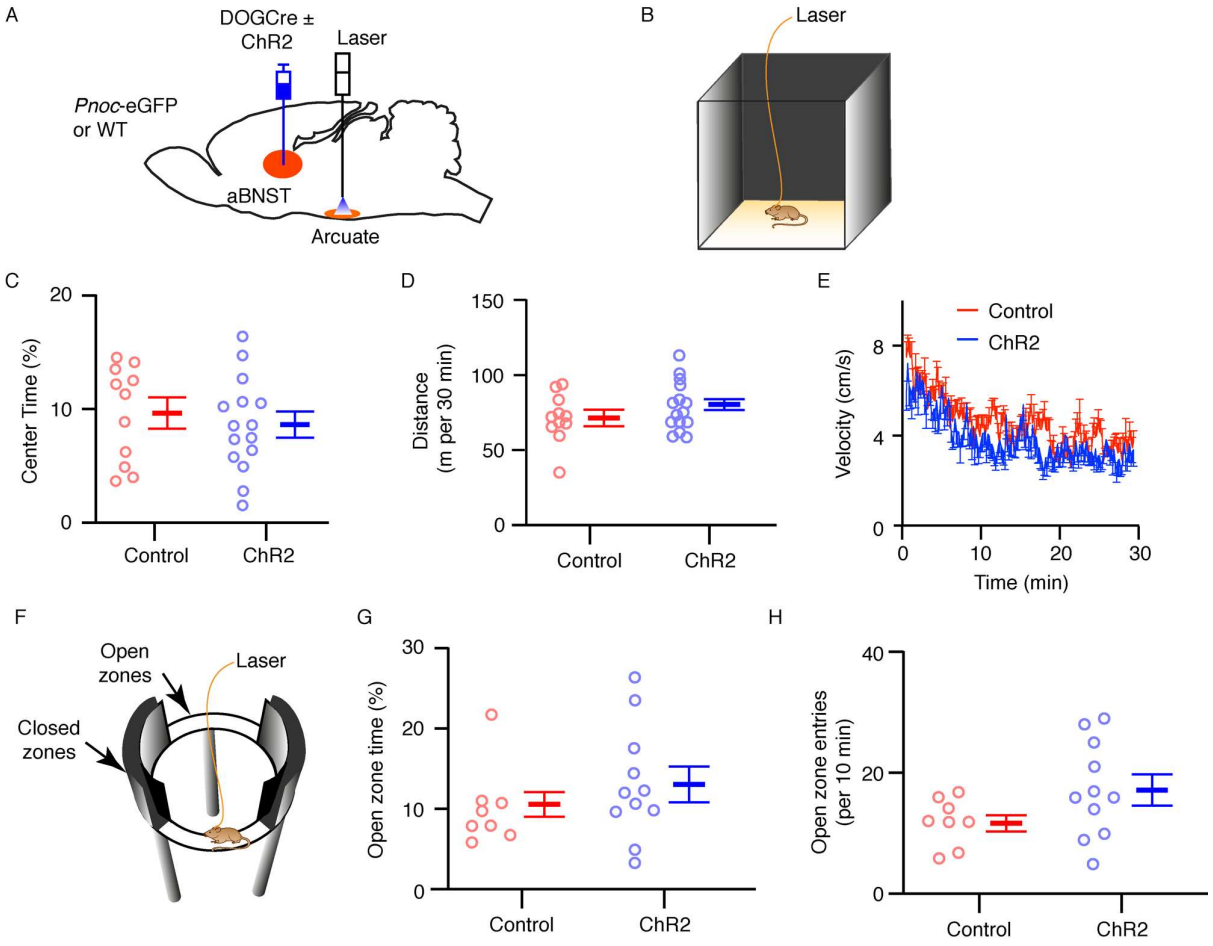

Figure 5. Optogenetic stimulation of aBNST nociceptin fibers in the arcuate nucleus does not induce anxiety-like behavior.

(**A**) Line diagram of *Pnoc*-eGFP mice and wild-type (WT) littermate controls injected with DOGCre ± ChR2-mCherry AAVs into the aBNST and optical fibers implanted into the arcuate nucleus. (**B**) Schematic representation of mice tethered to a 470 nm laser and photostimulated (3 s 10 Hz bursts every 4 s) for 30 minutes in a novel open-field arena. (**C**-**E**) Percentage time spent in the center (**C**, unpaired t-test, t (24) = 0.63, p = 0.53), total distance travelled (**D**, unpaired t-test, t (24) = 1.20, p = 0.24) and mouse velocity (**E**, 2-way RM ANOVA, Interaction: f (173,4152) = 1.08, p = 0.241; ChR2 expression: f (1,24) = 1.44, p = 0.241) in the open-field arena for mice expressing (blue, n = 15 mice) and not expressing (red, n = 11 mice) ChR2-mCherry. Mean ± SEM. (**F**) Schematic representation of mice tethered to a 470 nm laser

and photostimulated (3 s 10 Hz bursts every 4 s) for 10 minutes on a novel elevated-zero maze. (**G** and **H**) Percentage time in (**G**, unpaired t-test, $t(17) = 0.99$, $p = 0.33$) and entrances (**H**, unpaired t-test, $t(17) = 1.74$, $p = 0.10$) to the anxiogenic open zones in mice expressing (blue, n = 11 mice) and not expressing (red, n = 8 mice) ChR2-mCherry. Data is expressed as mean ± SEM.

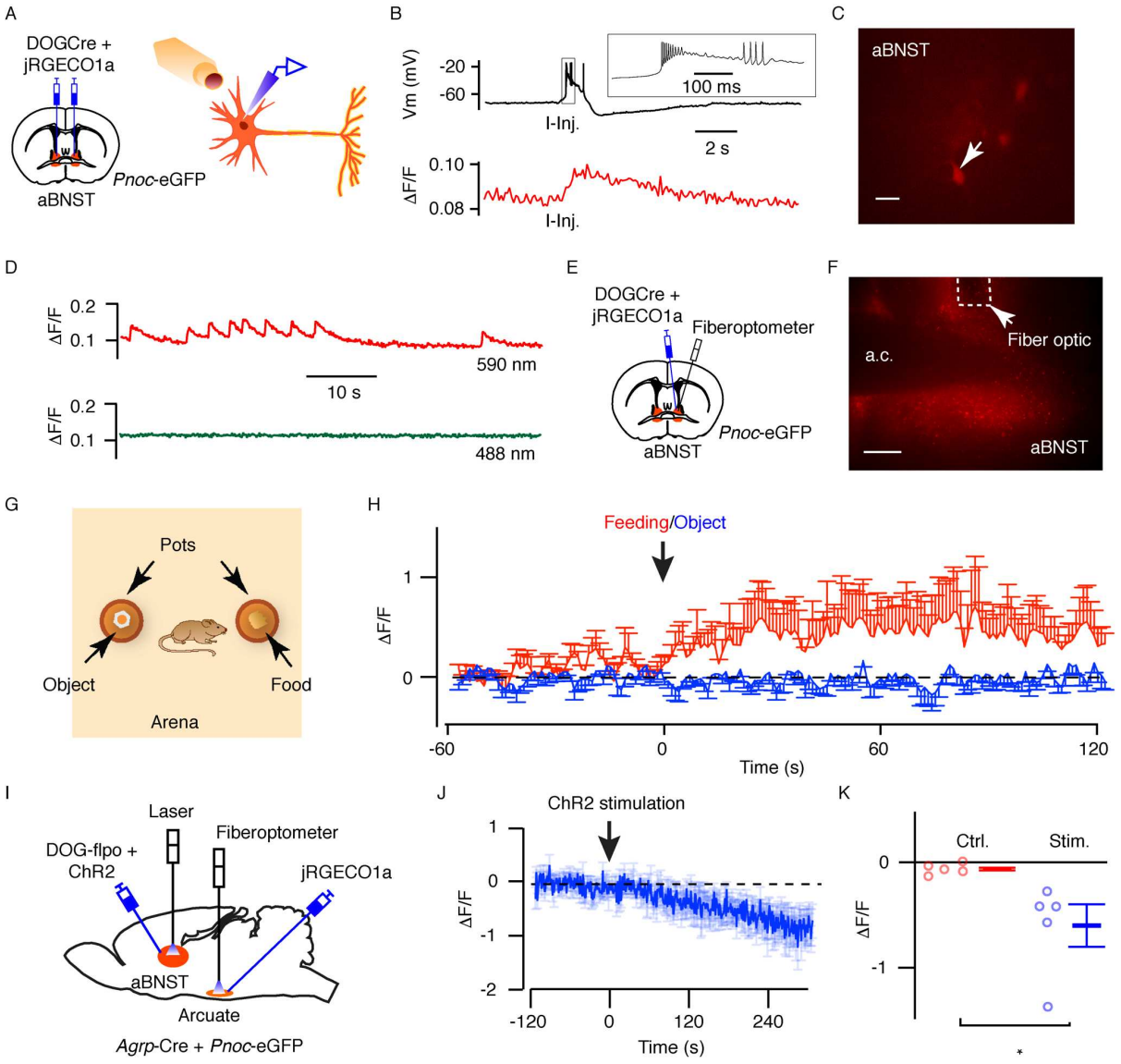

Figure 6. Activity of aBNST nociceptin neurons increases during the initiation of feeding.

(**A**) Diagram of *Pnoc*-eGFP mice injected with DOGCre and jRGECO1a AAVs into the aBNST for ex vivo imaging and recording. (**B**) Simultaneous measurement of electrical excitability (top) and florescence intensity (ΔF/F, bottom) in aBNST jRGECO1a-expressing neurons (n = 3). Action potential firing was evoked by depolarizing current injections (I-Inj.) and correlated with increased florescence. (**C** and **D**) Image of aBNST neuron (**C**) and corresponding changes in spontaneous jRGECO1a florescence (ΔF/F, **D**) at 590 nm but not 488 nm (n = 5). (**E**) Diagram of *Pnoc*-eGFP mice injected with DOGCre and jRGECO1a AAVs into the aBNST with optical fibers implanted in the aBNST. (**F**) jRGECO1a expression in the aBNST and optical fiber

location. (**G**) Diagram of open-field arena containing 2 pots (with a novel object or food). (**H**) Florescence intensity ($\Delta F/F$) in mice approaching a novel object (blue) or initiating feeding (red). Mean ± SEM. N = 7 mice. 2-way RM ANOVA (Interaction: $f(239,2868) = 1.44$, $p < 0.0001$; time: $f(239,2868) = 1.35$, $p < 0.001$; feeding vs object: $f(1,12) = 2.70$, $p = 0.14$). (**I**) Diagram of intercrossed *Pnoc*-eGFP and *Agrp*-Cre mice injected with DOG-flpo and flp-dependent ChR2-mCherry AAVs into the aBNST and cre-dependent jRGECO1a AAV into the arcuate nucleus. Optical fibers were placed in the aBNST for ChR2-stimulation and in arcuate nucleus for jRGECO1a activity recording. (**J**) Florescence intensity ($\Delta F/F$) in AgRP neurons before and following aBNST photostimulation, where indicated. Mean ± SEM. N = 5 mice. (**K**) AgRP activity ($\Delta F/F$) for mice shown in (**J**) before (ctrl.) and after stimulation (stim.). Mean ± SEM, * $p < 0.05$ (paired t-test, $t(4) = 2.97$, $p = 0.041$). Scale bars are 20 μm in (**C**) and 200 μm in (**F**). a.c., anterior commissure.

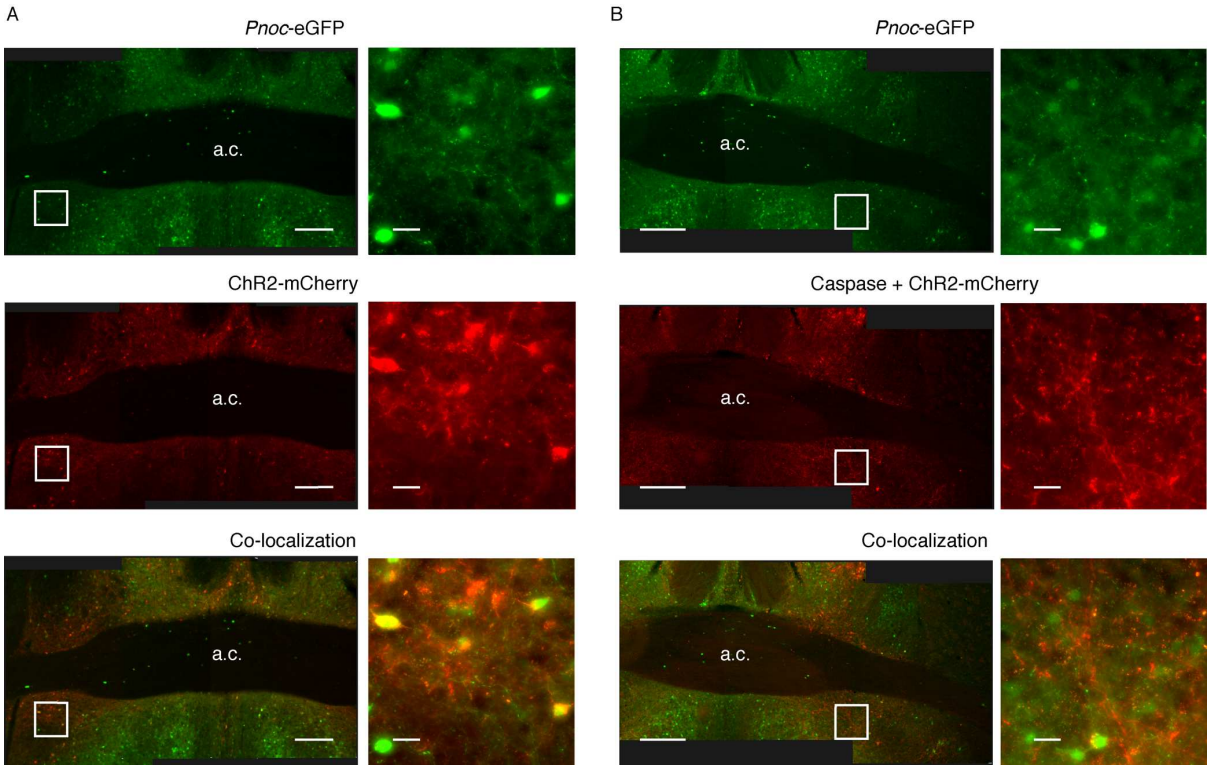

Figure 7. Caspase-mediated ablation of aBNST nociceptin neurons.

(**A** and **B**) Low magnification mosaic images (left) and expanded sections (right) from mice not expressing (**A**, n = 4) and expressing (**B**, n = 7) caspase-3 in aBNST *Pnoc* neurons. Images show eGFP expression driven by *Pnoc* promoter (top panels), cre-dependent expression of ChR2-mCherry (middle panels) and co-localization (bottom panels). Scale bars are 200 μm for low and 20 μm for high magnification images. a.c., anterior commissure.

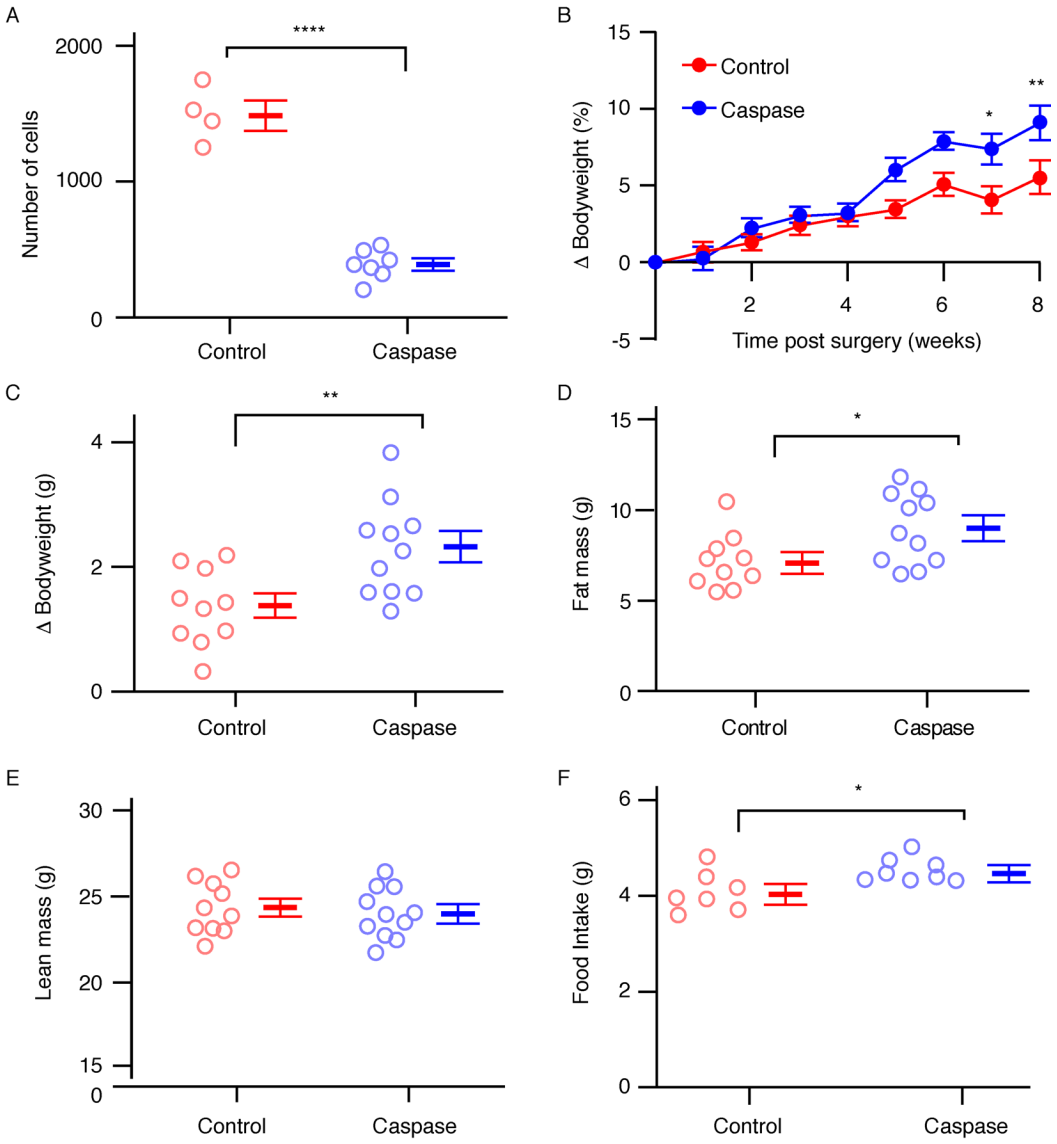

Figure 8. Loss of aBNST *Pnoc* neurons increases adiposity and bodyweight.

(**A**) Number of mCherry-expressing aBNST somas in control (red, n = 4 mice) and caspase-3-treated (blue, n = 7 mice) mice. Mean ± SEM, **** p<0.0001 (unpaired t-test, t (9) = 11.88, p = $4.19e^{-7}$). (**B**) Cumulative change in bodyweight (percentage of pre-surgery weight) in control (red, n = 10) and caspase-3 treated (blue, n = 11) mice. Mean ± SEM. 2-way RM ANOVA (Interaction: f (8,152) = 3.37, p = 0.0014; control vs caspase: f (1,19) = 5.02, p = 0.037). Sidak post-hoc test, * p<0.05, ** p<0.001. (**C**) Change in bodyweight 6 weeks post-surgery in control (red, n = 10 mice) and caspase-3-treated (blue, n = 11 mice) mice. Mean ± SEM, ** p<0.01 (unpaired t-test, t (19) = 3.07, p = 0.0063). (**D** and **E**) Fat (**D**, unpaired t-test, t (19) = 2.43, p =

0.025) and lean (**E**, unpaired t-test, t (19) = 0.48, p = 0.63) mass 6 weeks post-surgery in control (red, n = 10 mice) and caspase-3-treated (blue, n = 11 mice) mice. Mean ± SEM, * p<0.05. (**F**) Ad-libitum food intake in control (red, n = 7 mice) and caspase-3-treated (blue, n = 8 mice) mice. Mean ± SEM, * p<0.05 (unpaired t-test, t (13) = 2.53, p = 0.025).

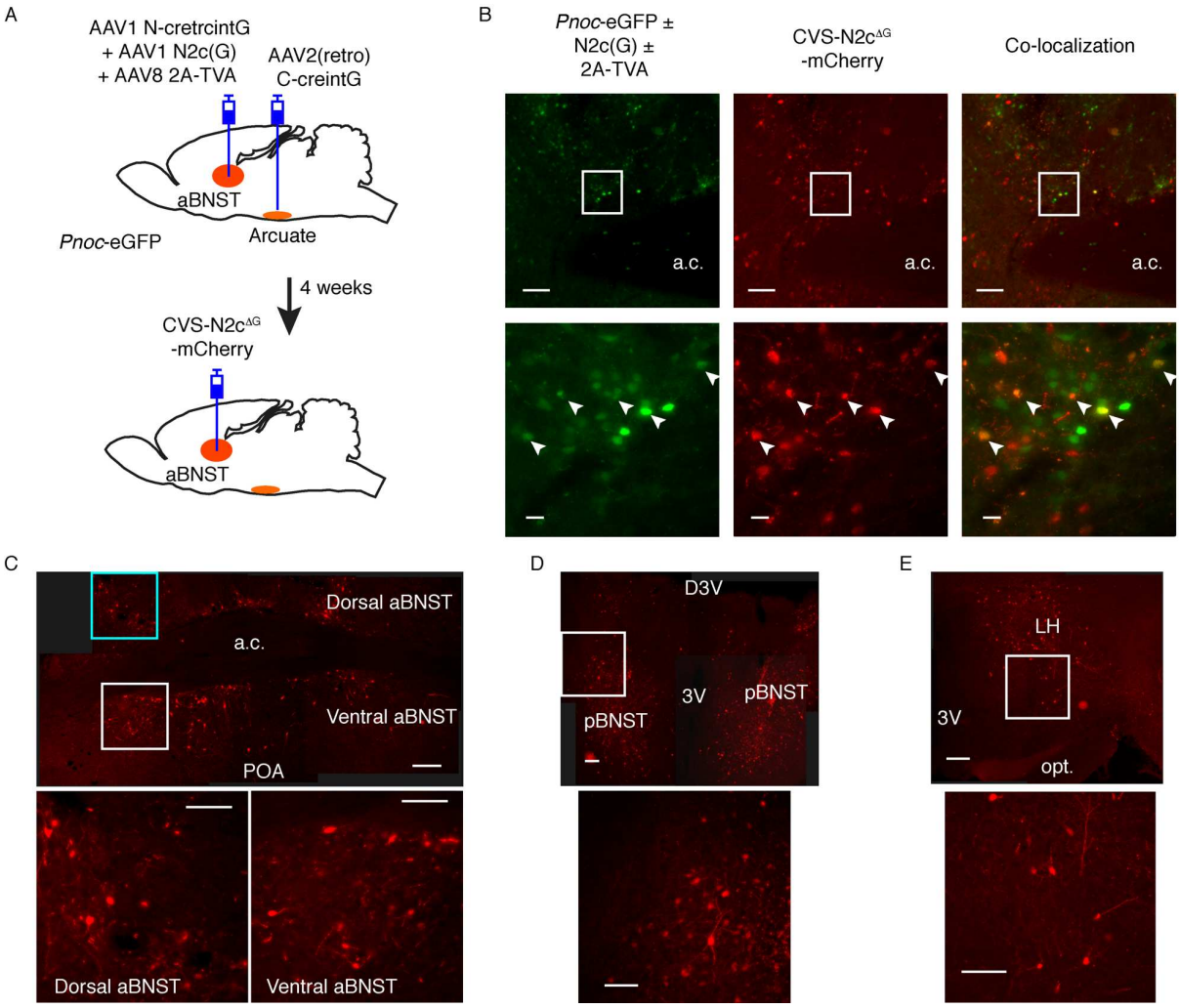

Figure 9. A population of aBNST *Pnoc* neurons receives inputs from the hypothalamus.

(**A**) Diagram of injection of C-creintG (serotyped with AAV2(retro)) into arcuate nucleus and N-cretrcintG (serotyped with AAV1) injected into aBNST of *Pnoc*-eGFP mice to drive cre-recombinase expression. A cre-dependent avian retroviral receptor (2A-TVA) tagged with GFP and N2c-glycoprotein (N2c(G)) tagged with GFP were simultaneously injected into aBNST. After 4 weeks to allow cre-dependent expression, a glycoprotein deficient rabies virus (CVS-N2c$^{\Delta G}$) expressing mCherry was injected into the aBNST. (**B**) Representative images (n = 3) of a coronal section containing eGFP expressing neurons driven by the *Pnoc* promoter and/or the tagged avian receptor and glycoprotein (left). Expression of mCherry driven by the rabies virus (middle) co-localizes (right) with a small number of GFP positive neurons (as shown by

the arrows). Scale bars are 200 μm for low magnification and 20 μm high magnification images corresponding to the boxed regions in upper panels. (**C**-**E**) Low magnification mosaic images (top) and expanded section (bottom) showing the expression of mCherry (n = 3 mice) driven by the rabies virus in presynaptic neurons in the aBNST (**C**), posterior BNST (**D**) and LH (**E**)**.** Scale bars are 200 μm for low and 100 μm and high magnification images. 3V, 3rd ventricle; a.c., anterior commissure; D3V, dorsal 3rd ventricle; LH, lateral hypothalamus; opt., optic tract; pBNST, posterior BNST; POA, preoptic area.